

Determination of Stabilization Time During Stress-Sensitivity Tests

by

Miao Yu

A thesis submitted in partial fulfillment of the requirements for the degree of

Master of Science

in

Petroleum Engineering

Department of Civil and Environmental Engineering

University of Alberta

© Miao Yu, 2021

ABSTRACT

Recent research shows that, the stress sensitivity of tight sandstone formations is significantly larger than that of high-permeability sandstone formations. Also, it takes a longer time for the permeability of a tight sandstone to get stabilized when it is subjected to a change in the confining stress. Such phenomenon is referred as the delayed stress sensitivity phenomenon. To quantify the delayed stress sensitivity phenomenon, a term called stabilization time can be used. It characterizes how much time is required for a given core to reach an unchanging permeability level when the confining pressure is changed from a lower pressure to a higher pressure. In this study, we make a hypothesis that the delayed stress sensitivity can be correlated with one or more pore-structure properties of the reservoir rocks. Stress-sensitivity tests on twelve tight cores are studied to testify the hypothesis that the stabilization time of tight sandstone cores under tri-axial stress test conditions can be related to the pore-structure properties of the reservoir rocks. Twelve cores with different permeability levels are retrieved from two field (i.e., a gas field and an oil field). Mercury intrusion porosimetry (MIP) tests and tri-axial stress-sensitivity tests have been conducted on these cores. The purpose of the MIP tests is to measure pore structure parameters such as the pore size distribution. Using a trial-and-error approach, we develop an empirical method to split the pores in a given core sample into large pores and small pores based on the pore size distribution charts. Once the pores are split into large pore and small pores, we can further calculate the area ratio of the large pores to the small pores. When conducting the tri-axial stress-sensitivity tests, we apply a constant axial stress of 10 MPa, but change the confining pressure from 5 to 30 MPa. During each tri-axial stress-sensitivity test, we monitor the variation of permeability versus time. By

analyzing the permeability variation data, we can determine the stabilization time, i.e., the time required for the permeability to reach a constant value when confining pressure changes to a higher level. We also record the cumulative stabilization time as a function of the confining pressure. The cumulative stabilization time (T) is found to linearly correlate with the logarithm function of the confining pressure ($\ln P$). We discover that the slope of the linear relationship between T and $\ln P$ shows a strong correlation with the area ratio of large pores to small pores. Regression using an inverse exponential function results in a regression coefficient of $R^2=0.86$. This indicates that a core sample with a larger area ratio of large pores to small pores has a shorter stabilization time, while a core sample with a smaller area ratio of large pores to small pores has a longer stabilization time. Such finding is in line with the physical understanding that the core sample with a smaller area ratio of large pores to smaller pores tends to have a steadier structure and deform more slowly than the one with a larger area ratio of large pores to smaller pores.

DEDICATION

This dissertation is dedicated to my parents, Mr. Haojie Yu and Mrs. Lichun Cui.

ACKNOWLEDGMENTS

First, I would like to express appreciation to my supervisor, Dr. Huazhou Li, for his dedication and support during my research. Also, I would like to thank Dr. Hai Huang at the Xi'an Shiyou University for his technical guidance and experimental support. Special thanks go to my thesis committee members for their insightful comments and suggestions on my thesis: Dr. Yong Li, Dr. Hongbo Zeng, and Dr. Zhehui Jin.

I gratefully acknowledge the financial support provided by one Natural Sciences and Engineering Research Council (NSERC) Discovery Grant as well as an Early Career Research Award to H. Li. Finally, I would like to thank Guangrong Lin and Dashan Shao for their assistance in conducting the stress-sensitivity tests.

TABLE OF CONTENTS

ABSTRACT.....	ii
DEDICATION.....	iv
ACKNOWLEDGMENTS.....	v
TABLE OF CONTENTS	vi
LIST OF TABLES	viii
LIST OF FIGURES	x
CHAPTER 1 INTRODUCTION.....	1
1.1. Research Background.....	1
1.2. Literature Review of Stress-Sensitivity of Reservoir Rocks	1
1.3. Problem Statement.....	3
1.4. Research Objectives.....	4
1.5. Thesis Structure	4
CHAPTER 2 EXPERIMENTAL PROGRAM	9
2.1. Materials	9
2.2. Equipment.....	10
2.3. Experimental Procedure.....	13
2.3.1. MIP Test Procedure	13
2.3.2. Stress-Sensitivity Test Procedure.....	14
CHAPTER 3 RESULTS AND DISCUSSION.....	15
3.1. MIP Test Results	15
3.2. Cumulative Stabilization Time as a Function of Confining Pressure.....	25
3.3. Final Permeability Loss and Total Stabilization Time.....	30
3.4. Dependence of Cumulative Stabilization Time on Area Ratio of Large Pores to Small Pores.....	32

CHAPTER 4 CONCLUSIONS AND RECOMMENDATIONS	37
4.1. Conclusions.....	37
4.2. Recommendations.....	38
BIBLIOGRAPHY	40
APPENDIX A: AN EXAMPLE CALCULATION SHOWING HOW TO PREDICT STABILIZATION TIME DURING STRESS-SENSITIVITY TESTS USING THE ESTABLISHED EMPIRICAL CORRELATIONS.....	44
APPENDIX B: DETAILED MIP TEST RESULTS.....	45

LIST OF TABLES

Table 1 Physical properties of the core samples used in this study.	9
Table 2 Results of the MIP test conducted on the core sample 8	16
Table 3 Estimated large-pore area, small-pore area, and area ratio of large pores to small pores of the 12 core samples.	25
Table 4 Regressed coefficients in Equation 2 for the 12 core samples.	29
Table 5 Results of the stress sensitivity tests conducted on the 12 core samples.	30
Table 6 Results of the MIP test conducted on the core sample 1	48
Table 7 Results of the MIP test conducted on the core sample 2	49
Table 8 Results of the MIP test conducted on the core sample 3	50
Table 9 Results of the MIP test conducted on the core sample 4	51
Table 10 Results of the MIP test conducted on the core sample 5	52
Table 11 Results of the MIP test conducted on the core sample 6	53
Table 12 Results of the MIP test conducted on the core sample 7	54
Table 13 Results of the MIP test conducted on the core sample 9	55
Table 14 Results of the MIP test conducted on the core sample 10	56
Table 15 Results of the MIP test conducted on the core sample 11	57

Table 16 Results of the MIP test conducted on the core sample 1258

LIST OF FIGURES

Figure 1 A simplified schematic showing the working mechanisms of the triaxial test systems.....	11
Figure 2 Triaxial core holder of the tri-axial test systems: (a) a digital picture; (b) a schematic showing its working mechanisms.	13
Figure 3 Plot of mercury intrusion pressure and mercury exit pressure versus mercury saturation measured by the MIP test conducted on the core sample 8.	17
Figure 4 Estimated pore size distribution and permeability contribution of the pores by the MIP test conducted on: (a) core 1, (b) core 2, (c) core 3, (d) core 4, (e) core 5, (f) core 6, (g) core 7, (h) core 8, (i) core 9, (j) core 10, (k) core 11, and (l) core 12.	24
Figure 5 Variation of permeability loss of core sample 3 as a function of time at different confining pressures: (a) 5 MPa, (b) 10 MPa, (c) 15 MPa, (d) 20 MPa, (e) 25 MPa, and (f) 30 MPa.....	28
Figure 6 Plots of the cumulative stabilization time versus confining pressure obtained for the 12 core samples.	29
Figure 7 Plots of permeability loss versus: (a) permeability; (b) porosity; (c) area ratio of large pores to small pores.	32
Figure 8 Plots of the slope of the cumulative stabilization time curve versus: (a) porosity; (b) permeability; (c) area ratio of large pores and small pores.	35

CHAPTER 1 INTRODUCTION

1.1. Research Background

During the production of reservoir fluids, the effective stress applied to a given formation increases as pore pressure reduces, causing the deformation of the formation structure. As a result, the porosity and permeability of the reservoir rock are reduced as the effective stress increases, which results in a decline in the production rate (Fatt and Davis, 1952; Mckee *et al.*, 1988; Iscan *et al.*, 2006). The experimental study conducted by Jose *et al.* (1997) indicated that the permeability loss of a tight formation could be as high as 90% under high effective stress levels. It is thus crucial to experimentally determine the stress sensitivity of a given reservoir rock to properly evaluate the impact of stress changes on the porosity and permeability of a reservoir rock.

1.2. Literature Review of Stress-Sensitivity of Reservoir Rocks

Many researchers have reported that stress sensitivity can exert a significant influence on the productivity of tight and shale formations (Liu *et al.*, 2011; Zhang *et al.*, 2014; Heidari *et al.*, 2015; Cao *et al.*, 2019; Wei *et al.*, 2019; Jiang *et al.*, 2020; Liu *et al.*, 2020; Zhang *et al.*, 2021a;b). For instance, Zhang *et al.* (2021) proposed a semi-analytical model to evaluate the transient pressure behavior of a multi-fractured horizontal well in a naturally fractured reservoir under the stress-sensitive effect. They found that stress sensitivity has a dominant impact on the transient pressure behavior in the intermediate-time and late-time flow periods. To better reveal the stress sensitivity of tight formations, many researchers have conducted stress-sensitivity tests, leading to the proposal of empirical

relations correlating the ultimate permeability losses with the effective stress applied. Jones *et al.* (1975) and Yin *et al.* (2006) developed empirical models that consider different levels of permeability loss and effective stress by using different function forms. Others relied on theoretical approaches to develop stress sensitivity models. Based on the grain packing model, Li *et al.* (2016) built a theoretical model that describes the dependence of permeability on effective stress, Poisson's ratios and Young's moduli. Ge *et al.* (2018) developed a stress sensitivity model that considers the dependence of permeability losses on the pore-structure parameters including pore radii and throat radii. Other researchers have also tried to unravel the relationship between stress sensitivity and pore-structure properties (Yang *et al.*, 2016; Zhang *et al.*, 2018). Another popular theory that is widely used in the study of deformation of porous medium is called the Hertz contact deformation theory proposed by Gangi *et al.* (1976). Based on the Hertz deformation theory, Liu *et al.* (2020) built a mathematical model that describes the relationship between permeability loss and effective stress. Pore-structure properties such as average pore radii were taken into account in their model.

Although there are many experimental and theoretical studies devoted to revealing the dependence of permeability losses on the effective stress and other parameters, little attention has been paid towards the dynamic change of permeability as a function of time when the effective stress is changed from a lower value to a higher one. The typical permeability-variation history during a stress-sensitivity test can be divided into two stages: a declining stage and an equilibrium stage. During the declining stage, the permeability declines until reaching the lowest value. After reaching the lowest value, it enters the equilibrium stage where the permeability remains unchanged. The time for the

permeability to enter the equilibrium stage can be defined as the stabilization time. In laboratory stress-sensitivity tests, a testing duration of 0.5 hour to 2 hours is normally adopted according to Petroleum Industry Standard of China (Zhu, 2002). But such duration may be insufficient because the required stabilization time for some tight core samples can be much longer than 2 hours. Nie *et al.* (2016) measured the permeability change as a function of time during the stress-sensitivity tests, finding that the stabilization time experienced by tight core samples can last up to 126 hours. Nie *et al.* (2016) developed an empirical correlation to describe the relationship between permeability loss and time. But they did not explore the underlying rock physical properties that may lead to the prolonged stabilization time of the tight core samples. The analytical study by Liu *et al.* (2020) suggests that pore-structure properties (such as the original pore radii and throat radii) exert a significant effect on the stress sensitivity of tight rocks.

1.3. Problem Statement

It is crucial for reservoir engineers to determine the permeability loss caused by the gradually decreasing effective stresses during the production period. A premature termination of the stress-sensitivity test will lead to an underestimation in the permeability loss. It is, thus, imperative to properly determine the stabilization time in a stress-sensitivity test. Furthermore, the underlying mechanisms leading to the prolonged stabilization times exhibited by some reservoir rocks are unknown, and need to be uncovered.

1.4. Research Objectives

This study attempts to investigate which physical property of a core sample plays a dominant role in affecting the stabilization time in stress-sensitivity tests. We make a hypothesis that the stabilization time can be correlated with one or more pore-structure properties of the reservoir rocks. Twelve tight cores with different permeability levels are retrieved from two fields (i.e., a gas field and an oil field). Mercury intrusion porosimetry (MIP) tests and tri-axial stress-sensitivity tests are to be conducted on these cores. The purpose of the MIP tests is to obtain macroscopic pore-structure features. When conducting the tri-axial stress-sensitivity tests, we apply a constant axial stress of 10 MPa, but change the confining pressure from 5 MPa to 30 MPa. During each tri-axial stress-sensitivity test, we monitor the variation of permeability versus time. By analyzing the permeability variation data, we can determine the stabilization time, i.e., the time required for the permeability to reach a constant value. We also record the cumulative stabilization time as a function of the confining pressure. Analysis of the experimental data can help reveal which parameter plays a dominant role in affecting the stabilization time of a given rock during the stress-sensitivity test.

1.5. Thesis Structure

The thesis contains four chapters:

- **Chapter 1** introduces the research background, literature review, problem statement, research objectives, and thesis structure.
- **Chapter 2** presents the experimental program employed in this thesis, including materials, equipment, and experimental procedure.

- **Chapter 3** is the main chapter. It presents the MIP test results and stress-sensitivity test results.
- **Chapter 4** summarizes the conclusions of this study and gives recommendations for future work.

References

Cao, N., Lei, G. Stress sensitivity of tight reservoirs during pressure loading and unloading process. *J. Petrol. Explor. Dev.* 2019, **46** (1): 132-138.

Fatt, I., Davis, D.H. Reduction in permeability with overburden pressure. *J. Pet. Tech.* 1952, **4** (12): 16.

Gangi, A.F. Hertz theory applied to the porosity-pressure, permeability-pressure and failure strength-porosity variations of porous rocks. ARMA-76-0119, 1976.

Ge, J., Jerath, S., Ghassemi, A., Ling, K. Sensitivity study on the poroelastic and thermoelastic effects on the stress reversal nearby an existing hydraulic fracture. ARMA-2018-287, 2018.

Heidari Sureshjani, M., Clarkson, C.R. An analytical model for analyzing and forecasting production from multifractured horizontal wells with complex branched fracture geometry. *SPE Res Eval & Eng.* 2015, **18** (3): 356-374.

Iscan, A.G., Kok, M.V., Bagci, A.S. Estimation of permeability and rock mechanical properties of limestone reservoir rocks under stress conditions by strain gauge. *J. Pet. Sci. Eng.* 2006, **53** (1): 13-24.

- Jiang, L., Liu, J., Liu, T., Yang, D. Semi-analytical modeling of transient pressure behaviour for a fractured vertical well with hydraulic/natural fracture networks by considering stress-sensitive effect. *J. Nat. Gas Sci. Eng.* 2020. **82**: 103477.
- Jones, F.O. A laboratory study of effects of confining pressure on fracture flow and storage capacity in carbonate rocks. *J. Pet. Tech.* 1975, **27** (1): 21-27.
- Jose, G. Numerical simulation of coupled fluid-flow/geomechanical behavior of tight gas reservoirs with stress sensitive permeability. SPE-39055, 1997.
- Li, Y.D., Dong, P.C. Stress sensitivity analysis of permeability and threshold pressure gradient in low-permeability reservoirs. *Pet. Geol. Recovery Effi.* 2016, **23** (6): 57-63 (In Chinese).
- Liu, J., Jiang, L., Liu, T., Yang, D. Modeling tracer flowback behaviour for a fractured vertical well in a tight formation by coupling fluid flow and geomechanical dynamics. *J. Nat. Gas Sci. Eng.* 2020, **84**: 103656.
- Liu, K, Yin, D.Y., Sun, Y.H. The mathematical model of stress sensitivities on tight reservoirs of different sedimentary rocks and its application. *J. Pet. Sci. Eng.* 2020, **193**: 107372.
- Liu, R.J., Liu, H.Q. Study of stress sensitivity and its influence on oil development in low permeability reservoir. *J. Rock. Mech. Eng.* 2011, **30** (S1): 2697 (In Chinese).
- Mckee, C.R., Bumb, A.C, Koenig, R.A. Stress dependent permeability and porosity of coal and other geologic formations. *SPE Form. Eval.* 1988, **3** (1): 81-91.

- Nie, X.R, Wang, C.L, Liu, J. Experimental study on stress sensitivity for tight reservoirs based on time scale. *J. Unconv. Oil Gas* 2016, **3** (4): 22-24 (In Chinese).
- Wei, M., Duan, Y., Dong, M., Fang, Q., Dejam, M. Transient production decline behavior analysis for a multi-fractured horizontal well with discrete fracture networks in shale gas reservoirs. *J. Porous. Media.* 2019, **22** (3): 343-361.
- Yang, Y.F., Zhang, W.J., Gao, Y., Wan, Y.J., Su, Y.H., An, S.Y., Sun, H., Zhang, L., Zhao, J., Liu, L., Liu, P., Liu, Z., Li, A., Yao, J. Influence of stress sensitivity on microscopic pore structure and fluid flow in porous media. *J. Nat. Gas Sci. Eng.* 2016, **36**: 20-31.
- Yin, S.X., Wang, S.X. Effect and mechanism of stresses on rock permeability at different scales. *SCI China Ser. D.* 2006, **36** (5): 472-480.
- Zhang, W.T., Wang, Q., Ning, Z.H.F., Zhang, R., Huang, L., Cheng, Z.H.L. Relationship between the stress sensitivity and pore structure of shale. *J. Nat. Gas. Sci. Eng.* 2018, **59**: 440-451.
- Zhang, Y.H, Yang, D.Y. Evaluation of transient pressure responses of a hydraulically fractured horizontal well in a tight reservoir with an arbitrary shape by considering stress-sensitive effect. *J. Pet. Sci. Eng.* 2021, **202**: 108518.
- Zhang, Y.H, Yang, D.Y. Modeling transient pressure behaviour of a multi-fractured horizontal well in a reservoir with an arbitrary boundary and different fracture networks by considering stress-sensitive effect. *J. Hydrol.* 2021, **600**: 126552.

Zhang, Z., He, S., Liu, G., Guo, X., Mo, S. Pressure buildup behavior of vertically fractured wells with stress-sensitive conductivity. *J. Pet. Sci. Eng.* 2014, **122**: 48-55.

Zhu, B. Standard method for evaluating stress-sensitivity flow tests. Petroleum Industry Standard of China. 2002, SY/T 5358 (In Chinese).

CHAPTER 2 EXPERIMENTAL PROGRAM

2.1. Materials

In this study, a total of twelve natural sandstone core samples are used in the stress-sensitivity tests. Among them, five core samples are retrieved from a gas field, while seven core samples are retrieved from an oil field. Table 1 shows the physical properties of these twelve cores. It can be seen from Table 1 that the permeability of these cores varies over a large range (i.e., [0.0236 mD, 129.0900 mD]). The porosity of these cores also varies over a large range (i.e., [2.70%, 17.8%]).

Table 1 Physical properties of the core samples used in this study.

No.	Lithology	Depth, m	Permeability, mD	Porosity, %	Length, cm	Diameter, cm	Reservoir type
1	Sandstone	628.5	0.0236	4.10	3.428	2.428	Oil
2	Sandstone	648.7	0.0754	8.80	3.362	2.448	Oil
3	Sandstone	1936.6	0.0843	9.70	3.370	2.433	Oil
4	Sandstone	1208.0	129.0900	17.80	3.317	2.503	Oil
5	Sandstone	1348.1	10.9700	16.00	3.296	2.459	Oil
6	Sandstone	633.3	0.0524	6.50	3.388	2.428	Oil
7	Sandstone	628.93	0.0396	2.70	3.393	2.418	Oil
8	Sandstone	2876.8	0.4786	14.01	5.019	2.526	Gas
9	Sandstone	2876.6	0.4723	12.51	5.095	2.526	Gas
10	Sandstone	2914.9	0.9310	16.30	4.817	2.524	Gas
11	Sandstone	2916.1	0.9889	15.66	4.963	2.526	Gas
12	Sandstone	2877.1	0.4081	12.70	5.079	2.528	Gas

2.2. Equipment

2.2.1. MIP Apparatus

A MIP apparatus (AutoPore IV 9500, Micromeritics Instrument Corporation, Georgia, USA) is used to measure the pore size distributions of all the core samples. As a non-wetting fluid, mercury can be forced into a core sample by overcoming the capillary pressure. Mercury enters the larger pores first. As pressure increases, mercury gradually fills smaller and smaller pores. Upon the completion of the MIP test, an intrusion capillary-pressure curve can be obtained. The intrusion capillary-pressure curve can be used to further characterize the pore size distribution of the tested core.

2.2.2 Triaxial Test Apparatus

We have used two setups to conduct the triaxial tests. The core samples 8-12 are tested by the triaxial test system (Rock 600-50 VHT, Top Industrie Company of France, Paris, France), while the core samples 1-7 are tested by another triaxial testing system (PVC-200 System, Micromeritics Instrument Corporation, Georgia, USA). The working mechanisms of both triaxial test systems are similar and shown in **Figure 1**. Both triaxial test systems are equipped with a permeability measurement functionality.

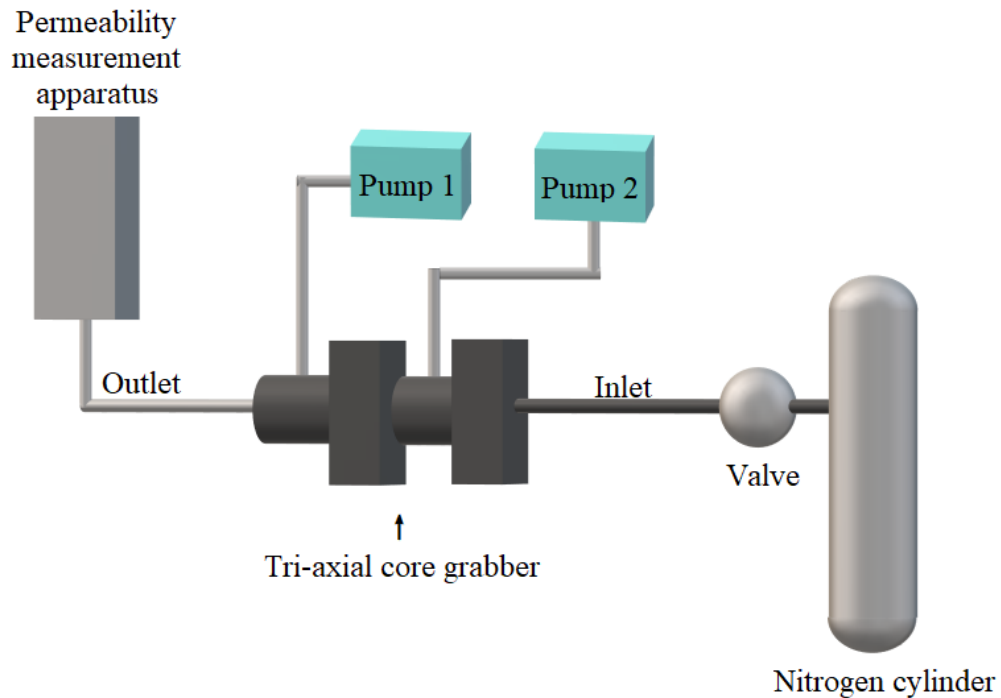
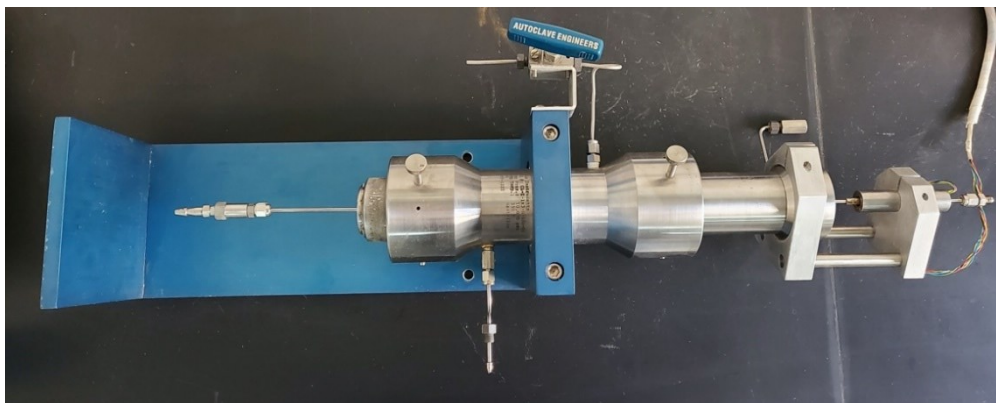


Figure 1 A simplified schematic showing the working mechanisms of the triaxial test systems.

As shown in Figure 1, a nitrogen cylinder is connected to the inlet of the tri-axial core grabber to supply a steady pore pressure. The permeability measurement apparatus is connected to the outlet of the tri-axial core grabber to measure the gas permeability. The tri-axial core grabber is designed to hold the core sample and apply tri-axial stresses. The working mechanisms of the tri-axial core grabber are shown **Figure 2**. As **Figure 2** shows, pump one is connected to the confining pressure cell. Once the pressure is applied, the confining pressure cell will be filled with water. This causes the rubber core grabber to deform and apply pressure to the core sample. Pump two is connected to the axial pressure cell. Once pressure is applied to the axial pressure cell, the piston inside the core holder will move against the core sample and apply an axial stress to the core sample. After applying confining pressure and overburden pressure, the valve is then opened, allowing gas nitrogen to enter the inlet of the device with a constant pressure. The permeability

measurement apparatus connected to the outlet of the core gripper is used to measure the permeability of the core sample under different confining pressures at different times. Then the measured permeability data can be analyzed to assess the stress sensitivity of the rock sample. The permeability of core samples is measured by two different setups. The first permeability measurement setup (Flowrate Meter, Yonghui Petroleum Instrument Company, Changzhou, China) is used to measure the permeability of the cores with high permeability (i.e., core samples 4 and 5). It measures the pressure difference caused by flowing nitrogen with a sensitive capillary tube. The pressure difference can be used to calculate the permeability of the core sample. The second apparatus is made in-house. It is designed to measure the permeability of the low-permeability core samples (i.e., core samples 1-3 and 6-12)). It is equipped with a high-precision test tube that gathers nitrogen that passes through the core sample and measures its volume. The volumes and pressure differences across the core sample are collected every 60 minutes. The collected data can then be inserted into Darcy's law to calculate the permeability of the core sample. The moment when the permeability stops changing is recorded as the stabilization time. After the measurement at a given confining pressure is completed, we raise the confining pressure to a higher level to start a new test.



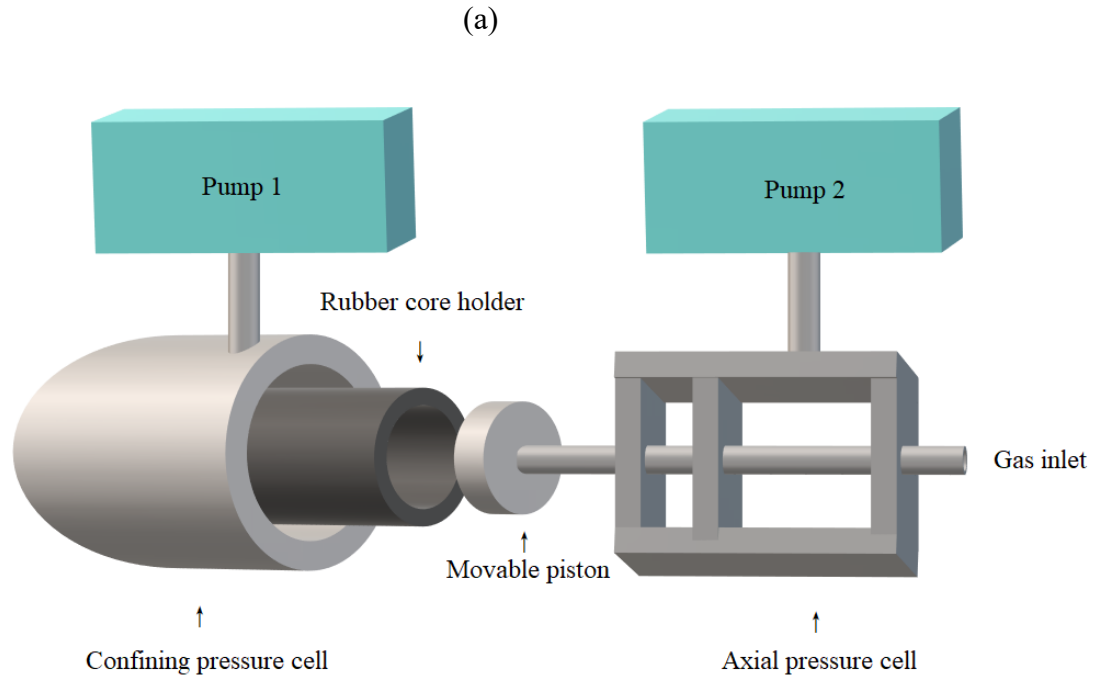


Figure 2 Triaxial core holder of the tri-axial test systems: (a) a digital picture; (b) a schematic showing its working mechanisms.

2.3. Experimental Procedure

2.3.1. MIP Test Procedure

First, all the core samples are carefully washed with an ethanol-benzene mixture with 75 vol% benzene to remove any formation fluid residue. Then the cores are kept being dried in an oven at 105°C until their weights remain unchanged. In the MIP test, we load a core sample into the core container in the MIP apparatus. We then seal the core container. Next, we open the nitrogen valve and activate the operating software. We then load the container into the high-pressure compartment and activate the device. Thereafter, the MIP apparatus start functioning and recording the data. Once the test is done and pressure is released, the core container is removed from the high-pressure compartment. We then close the nitrogen valve.

2.3.2. Stress-Sensitivity Test Procedure

In each stress-sensitivity test, we simulate the change of effective stress by maintaining constant overburden pressure and constant pore pressure while changing confining pressure. The axial pressure that simulates the overburden pressure is set to be 10 MPa. The confining pressure is set to be 5 MPa to 30 MPa with a 5 MPa increment. Prior to the stress sensitivity test conducted on each core sample, we measure the dimensions and weight of the core sample to be tested. We load the core sample into the triaxial test setup. After the core sample is secured, we apply a given confining pressure to the core sample using pump one. We then apply a constant axial pressure using pump two. After the confining pressure and axial pressure are applied, the inlet valve is opened to apply a constant pore pressure. Next, the permeability of the core sample is measured every 60 mins by using the permeability measurement apparatus. Once the permeability of the core sample stops changing, we deem that the test reaches the stabilization time. We then raise the confining pressure to the next level and repeat the same test procedure as mentioned above. After completing the entire test on the core sample, we first release the confining pressure by setting it to the atmospheric pressure. Next, we shut down the inlet valve, followed by releasing the axial pressure to the atmospheric pressure. Finally, the core sample is safe to be removed from the core grabber.

CHAPTER 3 RESULTS AND DISCUSSION

3.1. MIP Test Results

Using a capillary bundle model, Liu *et al.* (2020) derived a correlation that relates permeability to the pore radius and throat radius of a core sample:

$$k = \frac{n\pi r_p^4 r_t^4}{4\tau(r_p^4 + r_t^4)} = \frac{n\pi \left(\frac{r_p}{r_t}\right)^4}{4\tau \left[\left(\frac{r_p}{r_t}\right)^4 + 1\right]} = \frac{n\pi \left(\frac{A_p}{A_t}\right)^2}{4\tau \left[\left(\frac{A_p}{A_t}\right)^2 + 1\right]} \quad (1)$$

where k is permeability, n is the number of capillaries per unit cross-section area, τ is capillary tortuosity, r_p is pore radius, r_t is throat radius, A_p is pore's cross-section area, and A_t is throat's cross-section area. We can see from Equation 1 that the permeability of a core sample is closely related to the ratio of pore radius to throat radius, or equivalently, the pore-throat area ratio. As such, it is necessary to quantify the pore-throat area ratio of a given core sample, and check if the stabilization time is dependent on the pore-throat area ratio or not. However, we cannot infer the pore-throat area ratio of a given core sample using the MIP test results. We can obtain the pore size distribution of a given core sample using the MIP test results. Alternatively, we can roughly divide all the pores detected by a MIP test into large pores and small pores. Thereafter, we can then evaluate the area ratio of large pores over small pores. With this in mind, we develop an empirical method for identifying large pores and small pores based on the pore size distribution measured by a MIP test.

Basically, a typical MIP test measures the relationship between mercury saturation and mercury intrusion pressure. Based on such relationship, the software installed in the MIP

apparatus can be run to estimate the following parameters corresponding to a given mercury saturation: the pore size, permeability contribution of the pores with the average pore size, the frequency of the pore size, and the pore area. We have conducted MIP tests on all the core samples used in this study. Using the core sample 8 as an example, **Table 2** summarizes the results of a typical MIP test. **Figure 3** plots mercury intrusion pressure and mercury exit pressure versus mercury saturation measured by the MIP test conducted on the core sample 8. **Figure 4** shows the estimated pore size distribution and permeability contribution of the pores by the MIP test conducted on all the 12 core samples.

Table 2 Results of the MIP test conducted on the core sample 8

No.	Pore size, μm	Mercury saturation, %	Permeability contribution, %	Frequency, %	Pore area, μm^2
1	193.9161	0.0000	0.0000	0.0000	0.0000
2	100.2897	0.0000	0.0000	0.0000	0.0000
3	62.6155	0.0000	0.0000	0.0000	0.0000
4	40.1018	0.0000	0.0000	0.0000	0.0000
5	25.2853	0.0000	0.0000	0.0000	0.0000
6	15.7881	0.0000	0.0000	0.0000	0.0000
7	9.9392	0.0000	0.0000	0.0000	0.0000
8	6.1353	0.0000	0.0000	0.0000	0.0000
9	4.1416	0.0000	0.0000	0.0000	0.0000
10	2.6299	0.8127	9.2609	0.8127	5.6210
11	1.6306	7.6042	30.7870	6.7915	18.0583
12	1.0296	28.2658	36.3785	20.6615	21.9034
13	0.6338	55.8743	19.1071	27.6085	11.0913
14	0.4087	69.8458	3.7622	13.9715	2.3340

15	0.2540	74.8949	0.5535	5.0491	0.3257
16	0.1638	77.4607	0.1109	2.5659	0.0688
17	0.0996	79.2335	0.0308	1.7727	0.0176
18	0.0624	80.2866	0.0069	1.0531	0.0041
19	0.0405	80.9445	0.0017	0.6579	0.0011
20	0.0252	81.3644	0.0005	0.4199	0.0003
21	0.0161	81.5482	0.0001	0.1838	0.0000
22	0.0099	81.5556	0.0000	0.0074	0.0000
23	0.0062	81.5556	0.0000	0.0000	0.0000
24	0.0037	81.5556	0.0000	0.0000	0.0000

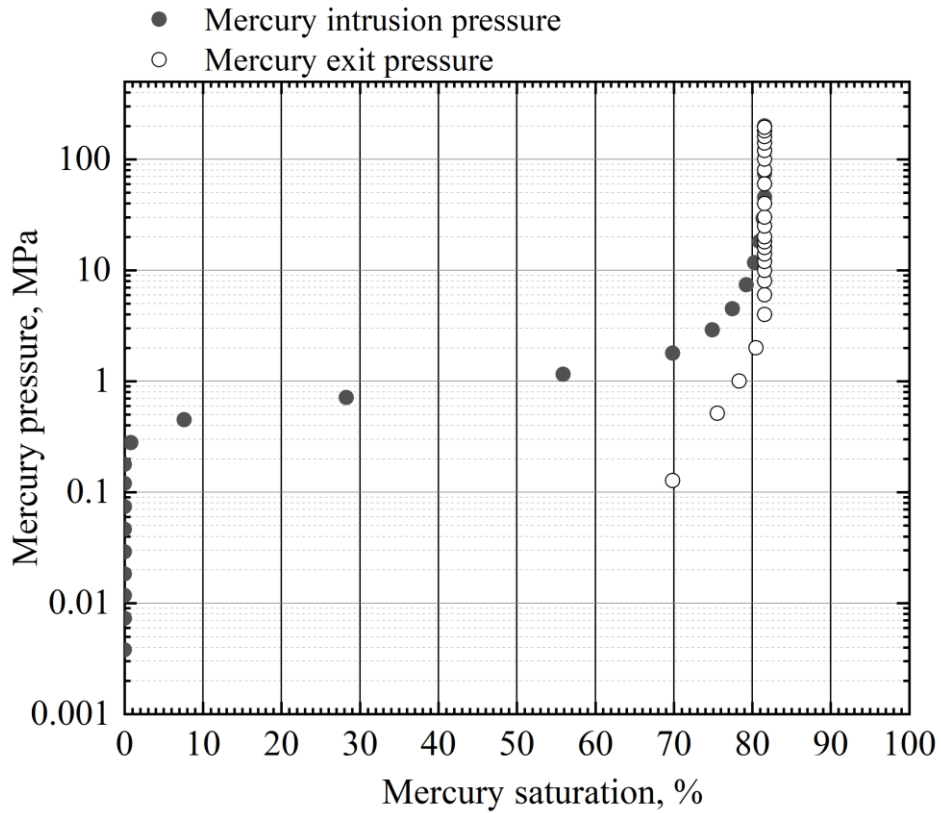
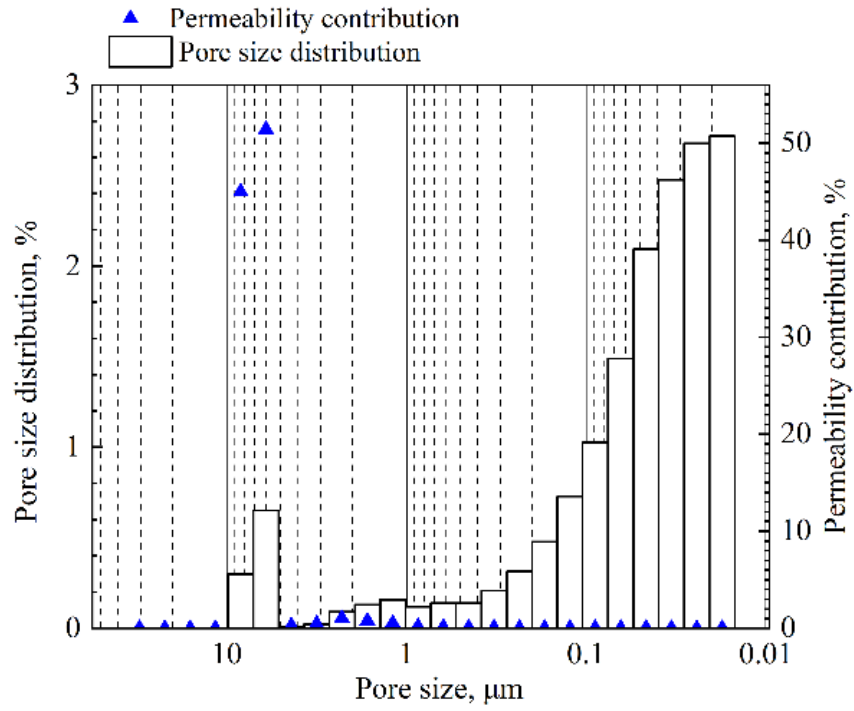
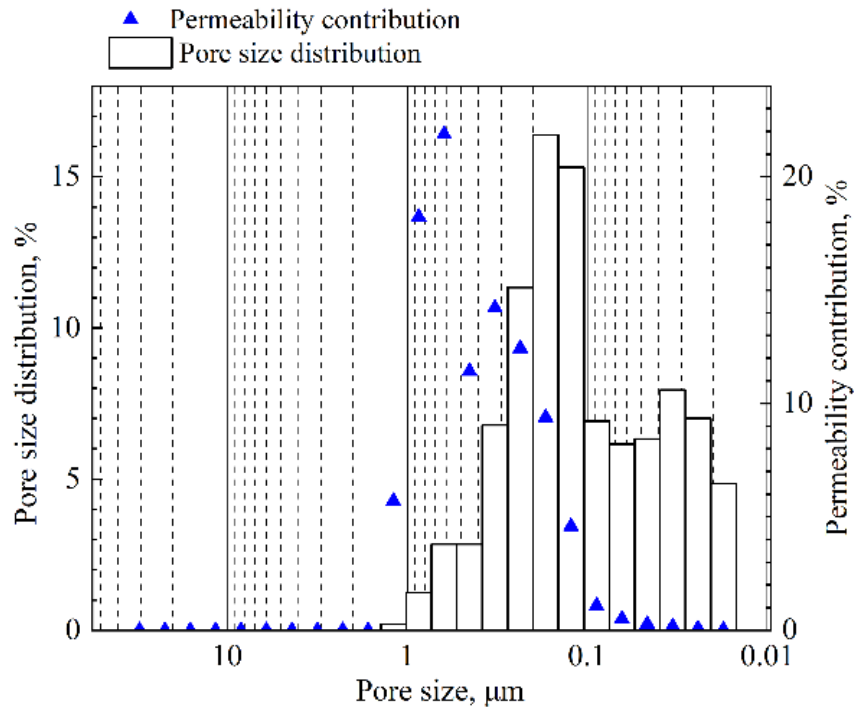


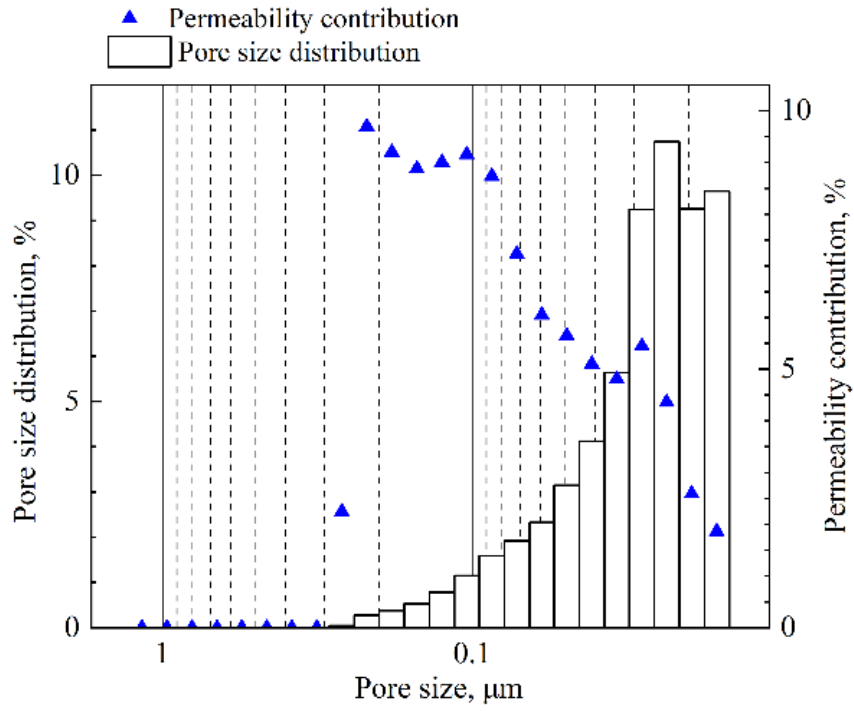
Figure 3 Plot of mercury intrusion pressure and mercury exit pressure versus mercury saturation measured by the MIP test conducted on the core sample 8.



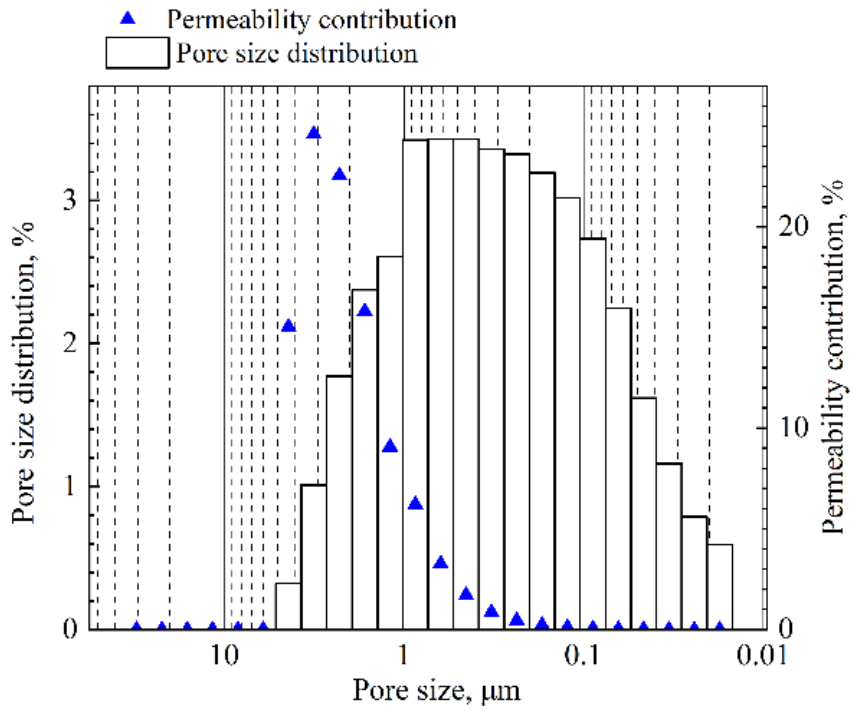
(a)



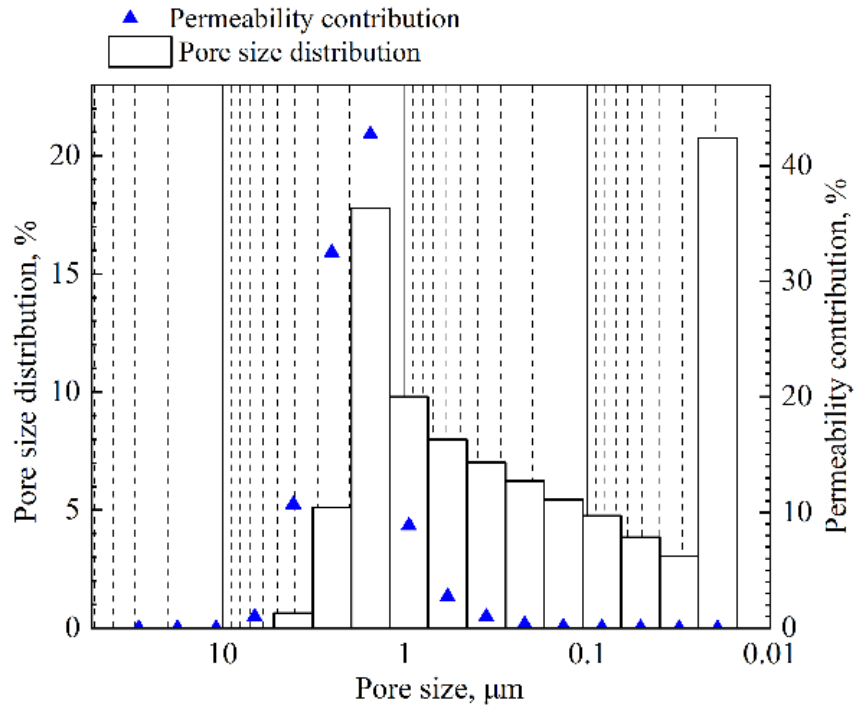
(b)



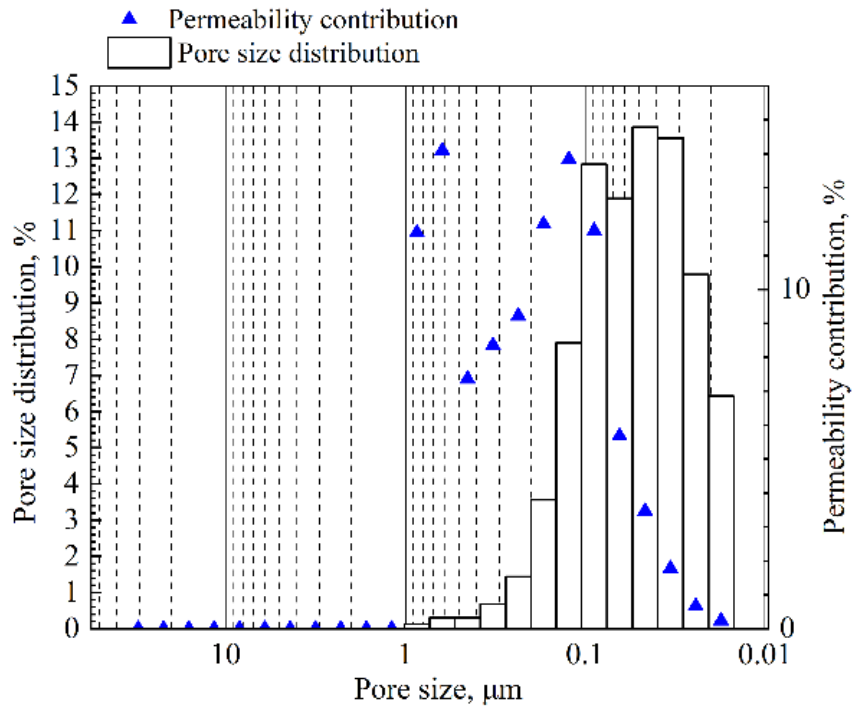
(c)



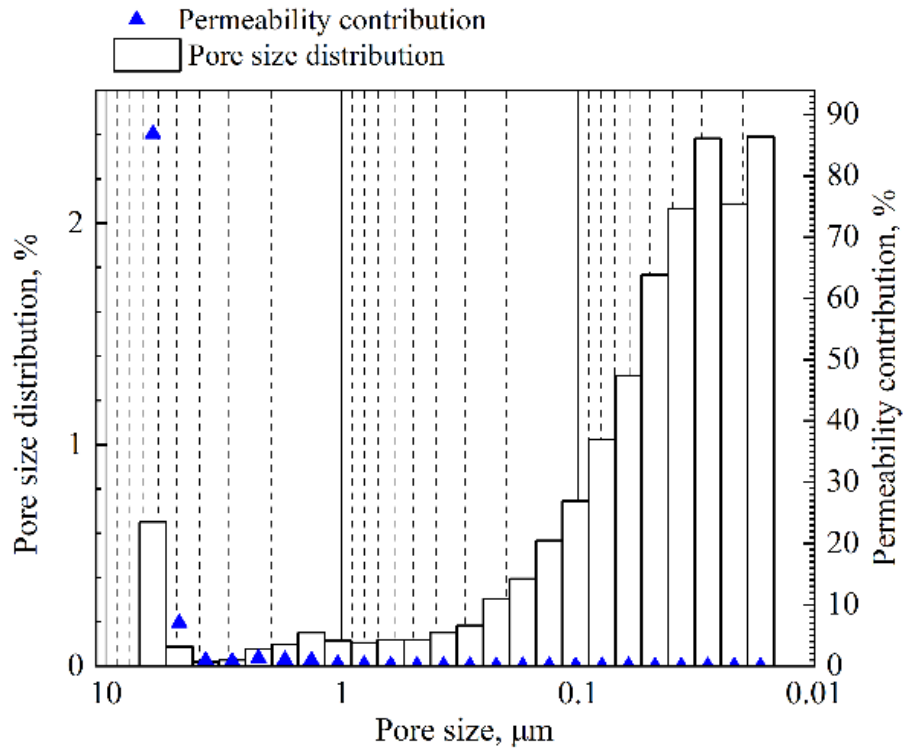
(d)



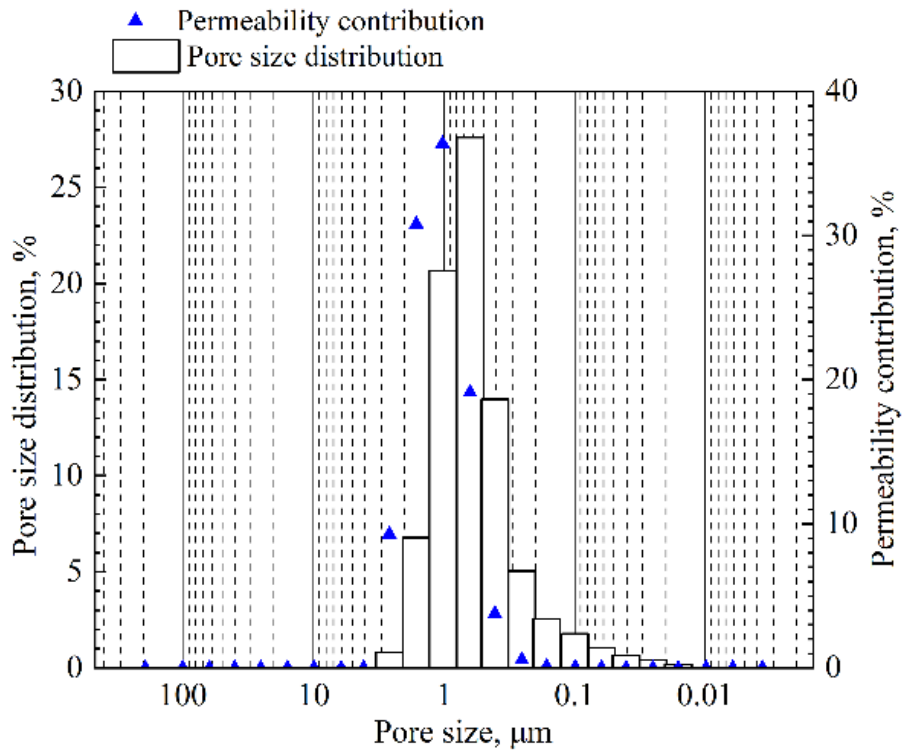
(e)



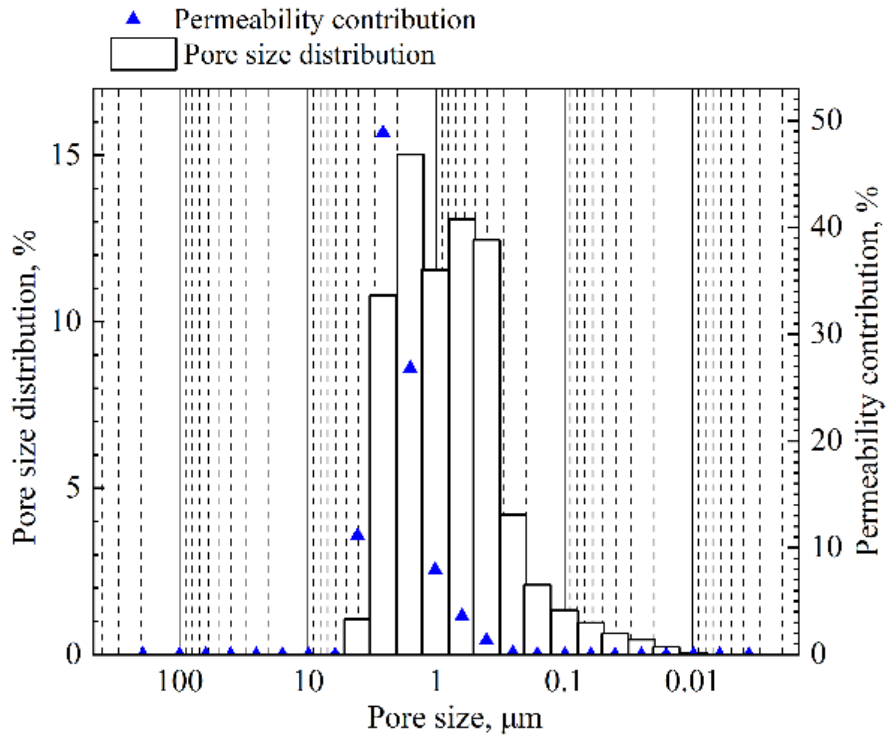
(f)



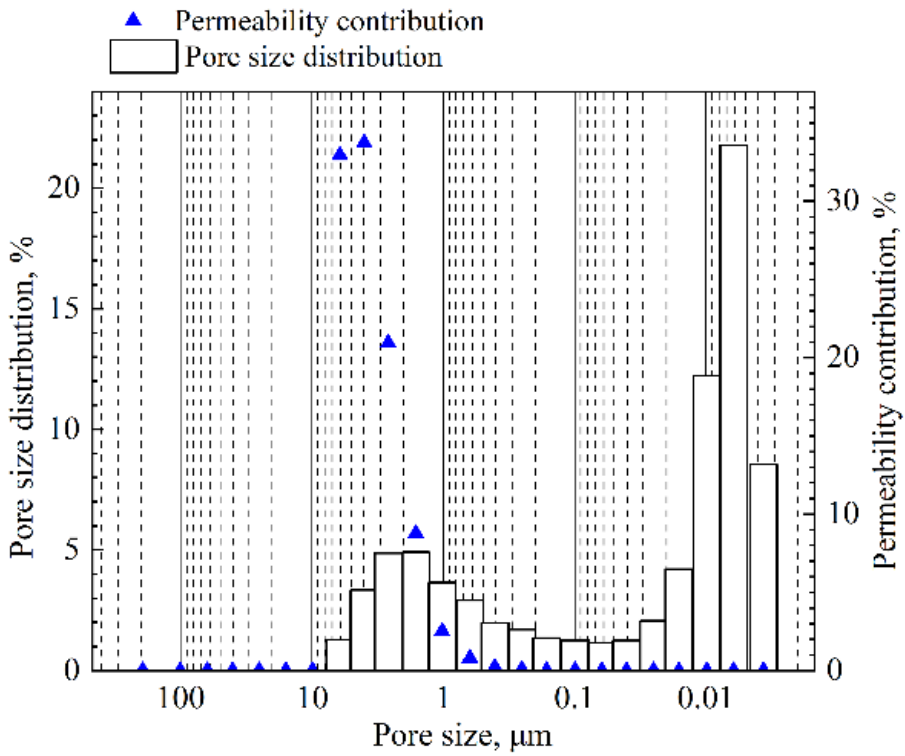
(g)



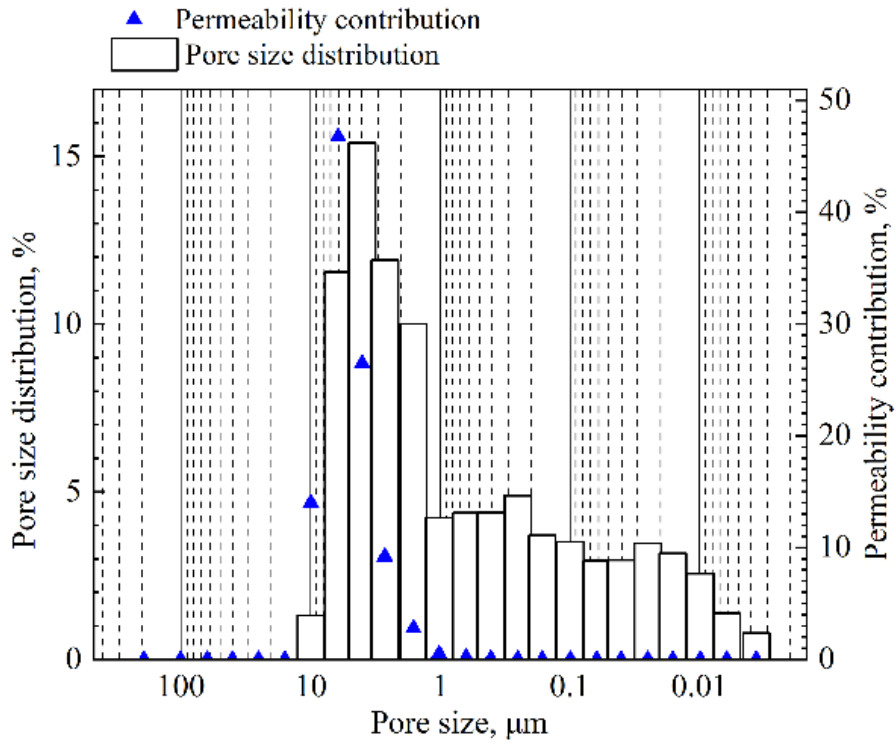
(h)



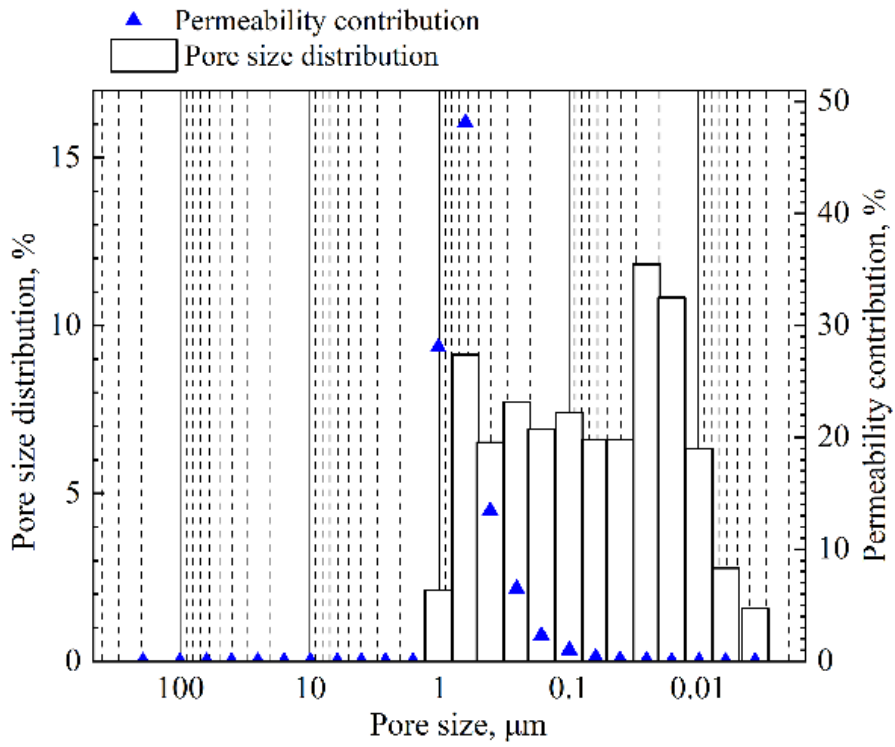
(i)



(j)



(k)



(l)

Figure 4 Estimated pore size distribution and permeability contribution of the pores by the MIP test conducted on: (a) core 1, (b) core 2, (c) core 3, (d) core 4, (e) core 5, (f) core 6, (g) core 7, (h) core 8, (i) core 9, (j) core 10, (k) core 11, and (l) core 12.

As seen from Equation 1, the permeability of a given porous medium is closely related to the pore-throat area ratio. But the MIP test results cannot provide the pore-throat area ratio. Here we propose an empirical method to divide the pores of a given core to large pores and small pores. The large pores can be considered as pores, while the small pores can be considered as throats. We can then approximate the pore-throat area ratio using the area ratio of large pores to small pores. It is noted that the following approach is purely empirical. It is selected based on multiple trials.

In general, the pore size distribution chart can exhibit two distinctive patterns. The first pattern corresponds to a unimodal pore size distribution as observed for core samples 2, 3, 4, 6, 8, 9, 11 and 12. For this pattern, we rely solely on the pore size distribution to define large pores and small pores. In this case, we group the pores with the highest frequency and any smaller pores into small pores. The remaining pores are classified as large pores.

The second pattern corresponds to a bimodal pore size distribution as observed for core samples 1, 5, 7, and 10. Let us take core sample 1 as an example to explain how larger pores and small pores are defined. As seen from Figure 4a, the pore size distribution chart of core sample 1 shows two peaks. The left peak of the pore size distribution chart is close to the permeability contribution chart. It can be concluded from Figure 4a that the larger pores close to the peak of the permeability contribution chart contribute more to the permeability of this core sample. In this case, the pores corresponding to the peak of the permeability contribution chart and any larger pores are grouped into large pores. The remaining pores are grouped into small pores.

After large pores and small pores of a given core sample have been properly defined, we use the following equation to evaluate the area ratio of large pores to small pores:

$$R = \frac{\sum_{i=1}^m \pi r_{li}^2 f_{li}}{\sum_{j=1}^n \pi r_{sj}^2 f_{sj}} \quad (1)$$

where R is the area ratio of the large pores to the small pores, r_s is the pore radius of a small pore, r_l is the pore radius of a large pore, f_s is the frequency of a small pore, f_l is the frequency of a large pore, m is the number of large pores, and n is the number of small pores. Table 3 summarizes the calculated large-pore area, small-pore area, and area ratio of large pores to small pores of the 12 core samples.

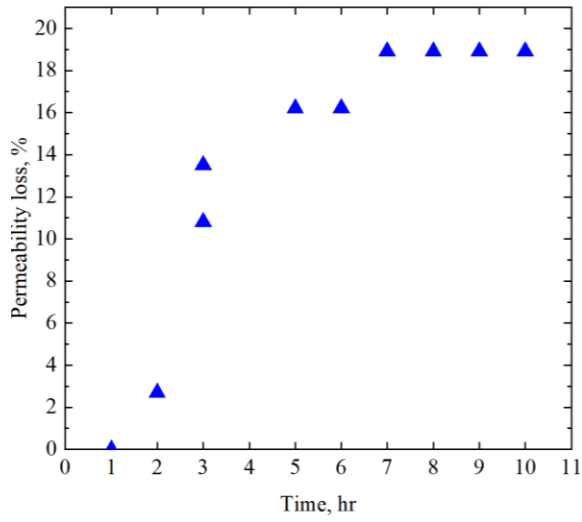
Table 3 Estimated large-pore area, small-pore area, and area ratio of large pores to small pores of the 12 core samples.

Core No.	Permeability, mD	Area of large pores, μm^2	Area of small pores, μm^2	Area ratio of large pores to small pores
1	0.0236	44.72218	1.661309	26.91984
2	0.0754	4.245924	0.815396	5.207191
3	0.0843	0.124636	0.012046	10.34665
4	129.09	38.22301	2.747502	13.91191
5	10.97	86.69657	12.95284	6.693246
6	0.0524	0.813358	0.053081	15.32303
7	0.0396	26.07485	3.937883	6.621541
8	0.4786	45.58274	13.84294	3.292851
9	0.4723	90.95935	57.797	1.573773
10	0.931	102.0897	51.95487	1.964969
11	0.9889	565.9818	365.5016	1.548507
12	0.4081	5.826263	1.877602	3.103035

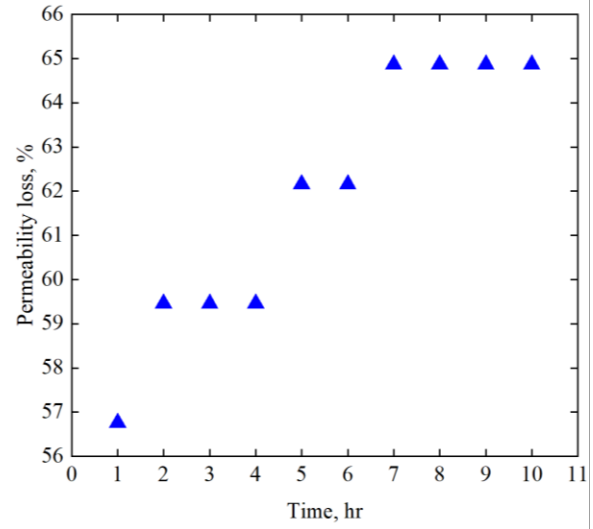
3.2. Cumulative Stabilization Time as a Function of Confining Pressure

In order to measure the stabilization time at a given confining pressure, we need to monitor the permeability change as a function of time. Permeability loss is used to quantify the

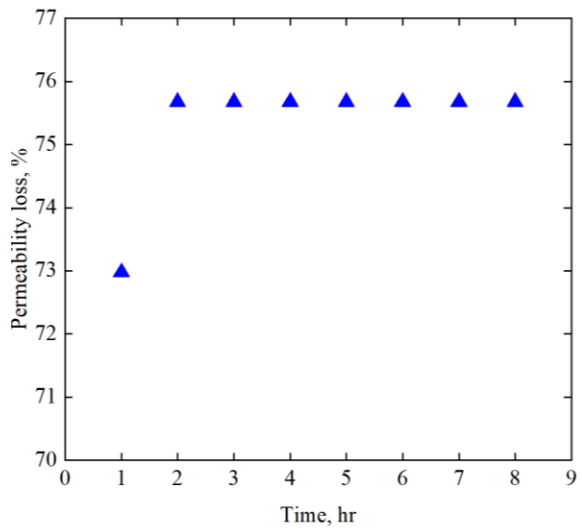
permeability change. It is calculated as the ratio of the difference between the original permeability and the current permeability to the original permeability. Taking the core sample 3 as an example, Figure 5 shows the variation in the permeability loss as a function of time at different levels of confining pressure. As seen from Figure 5, at a fixed confining pressure, the permeability loss first increases until reaching a constant value. The duration for the permeability loss to reach a constant value is deemed as the stabilization time.



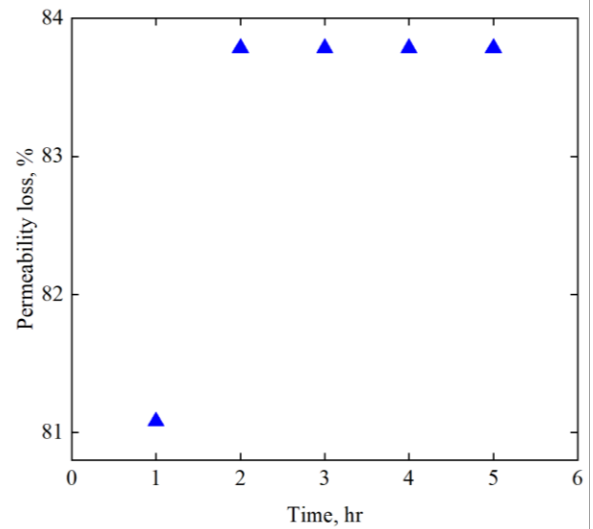
(a)



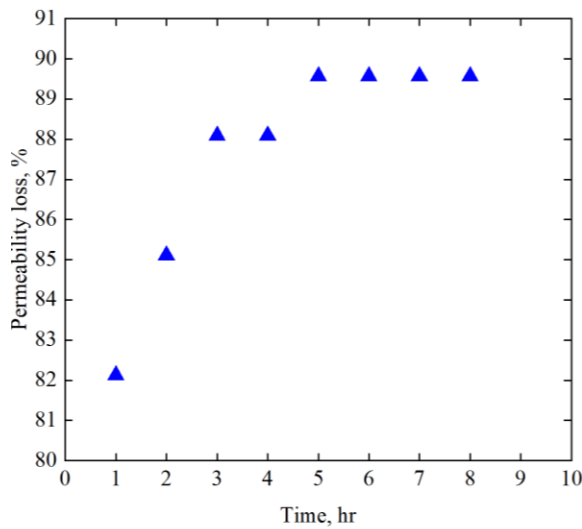
(b)



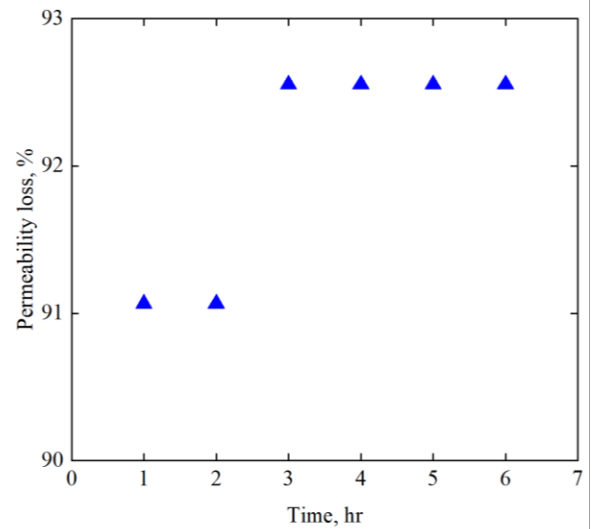
(c)



(d)



(e)



(f)

Figure 5 Variation of permeability loss of core sample 3 as a function of time at different confining pressures: (a) 5 MPa, (b) 10 MPa, (c) 15 MPa, (d) 20 MPa, (e) 25 MPa, and (f) 30 MPa.

Once the stabilization times at different confining pressures are obtained, we further plot the cumulative stabilization time against confining pressure. Figure 6 shows the plots of the cumulative stabilization time against confining pressure obtained for the 12 core samples. It can be seen from Figure 6 that different core samples exhibit different trend lines. For a given core sample, the cumulative stabilization time tends to increase with an increase in confining pressure. It is also discovered that the cumulative stabilization time measured for a given core sample shows a strong logarithmic relationship with confining pressure. The logarithmic relationship between the cumulative stabilization time and confining pressure is given by the following equation:

$$T = A \ln(P) + B \quad (2)$$

where T is the cumulative stabilization time, P is confining pressure, A and B are two coefficients to be determined by regressing the experimental data. Table 4 shows the regressed coefficients in Equation 2 for the 12 core samples.

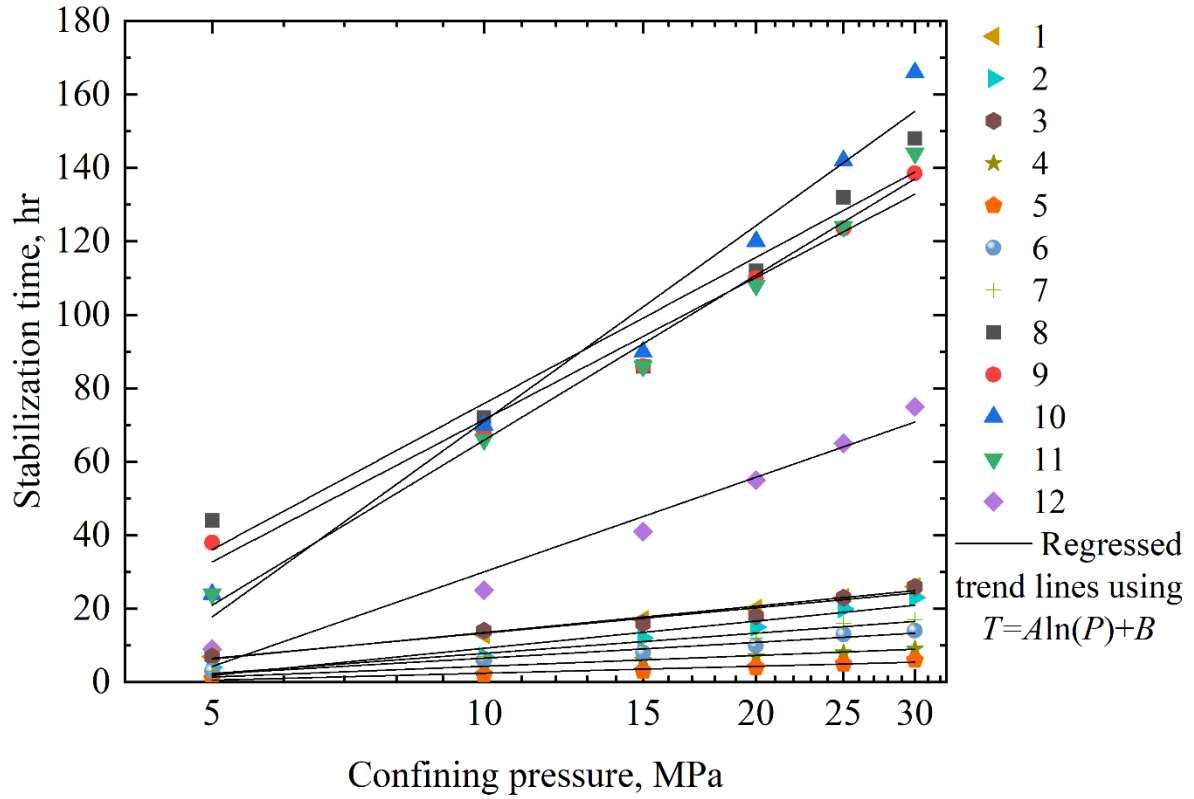


Figure 6 Plots of the cumulative stabilization time versus confining pressure obtained for the 12 core samples.

Table 4 Regressed coefficients in Equation 2 for the 12 core samples.

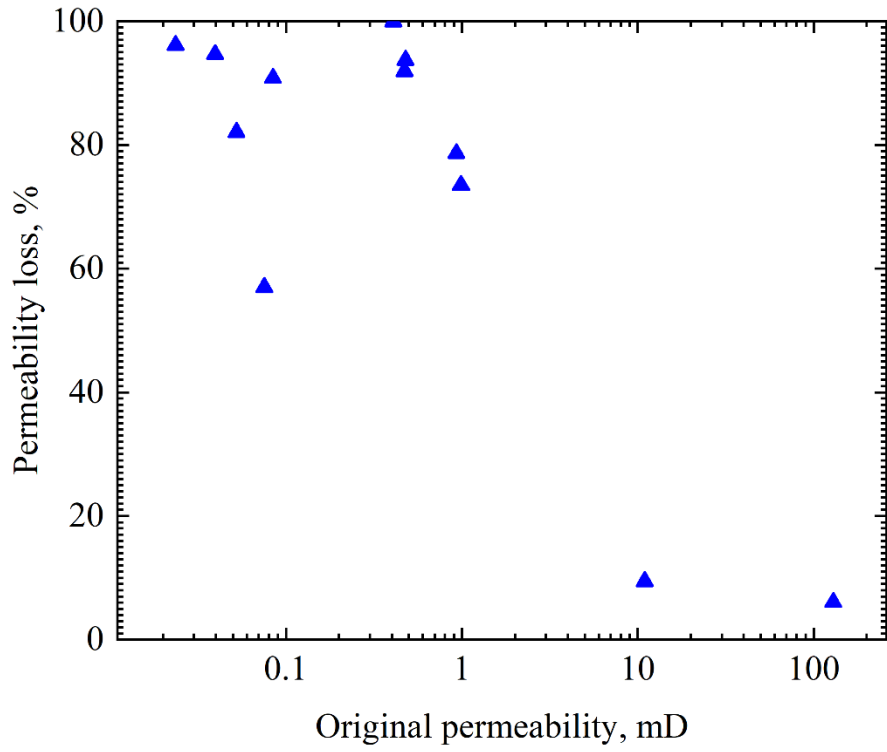
Core No.	A	B	R^2
1	10.377 ± 0.576	-10.413 ± 1.598	0.988
2	10.662 ± 1.505	-15.352 ± 4.174	0.926
3	9.928 ± 1.115	-9.5323 ± 3.092	0.952
4	4.230 ± 0.285	-5.447 ± 0.790	0.982
5	2.732 ± 0.356	-3.892 ± 0.988	0.936
6	6.197 ± 0.649	-7.768 ± 1.799	0.958
7	7.931 ± 0.668	-10.460 ± 1.852	0.972
8	57.360 ± 6.389	-56.215 ± 17.717	0.953
9	55.834 ± 3.969	-57.085 ± 11.004	0.980
10	76.812 ± 6.022	-105.852 ± 16.698	0.976
11	64.788 ± 3.450	-83.315 ± 9.566	0.989
12	37.143 ± 3.076	-55.509 ± 8.529	0.973

3.3. Final Permeability Loss and Total Stabilization Time

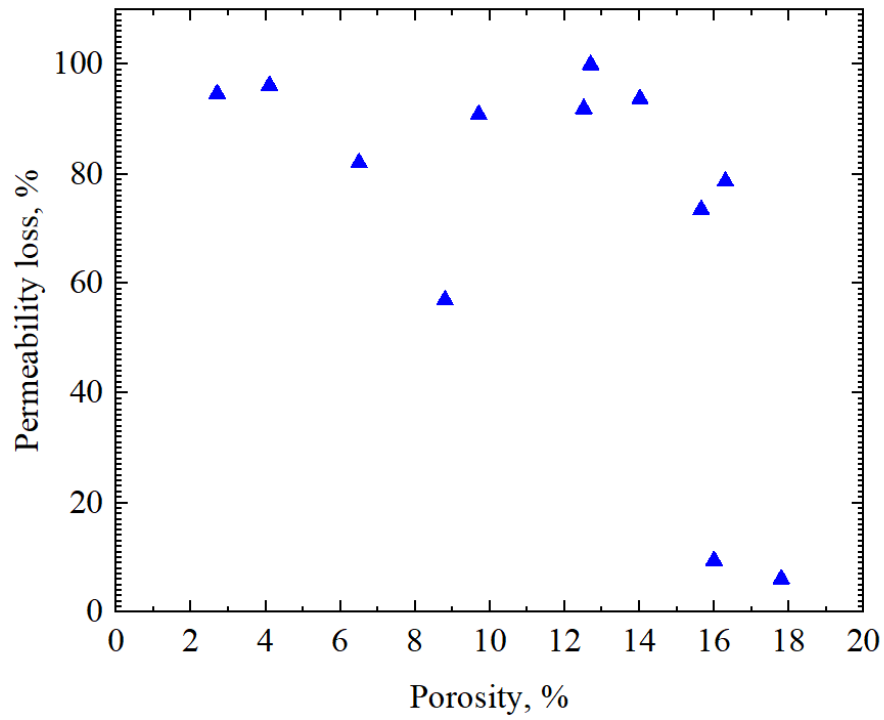
Table 5 summarizes the results yielded by the stress sensitivity tests conducted on the 12 core samples. Figure 7 further shows the plots of permeability loss versus the original permeability, porosity, and area ratio of large pores to small pores. As seen from Table 5 and Figure 7, in general, a core sample with a lower permeability tends to show a higher degree of permeability loss (i.e., a higher degree of stress sensitivity), and a shorter total stabilization time. But several exceptions exist. For instance, the core sample 4 shows a permeability loss of 6.07%, which is shorter than 9.42% shown by the core sample 5. This is in line with the fact that the core sample 4 has a higher permeability (i.e., 129.0900 mD) than the core sample 5 (i.e., 10.9700 mD). But the core sample 4 shows a total stabilization time of 9 h, which is longer than 6 hours shown by the core sample 5.

Table 5 Results of the stress sensitivity tests conducted on the 12 core samples.

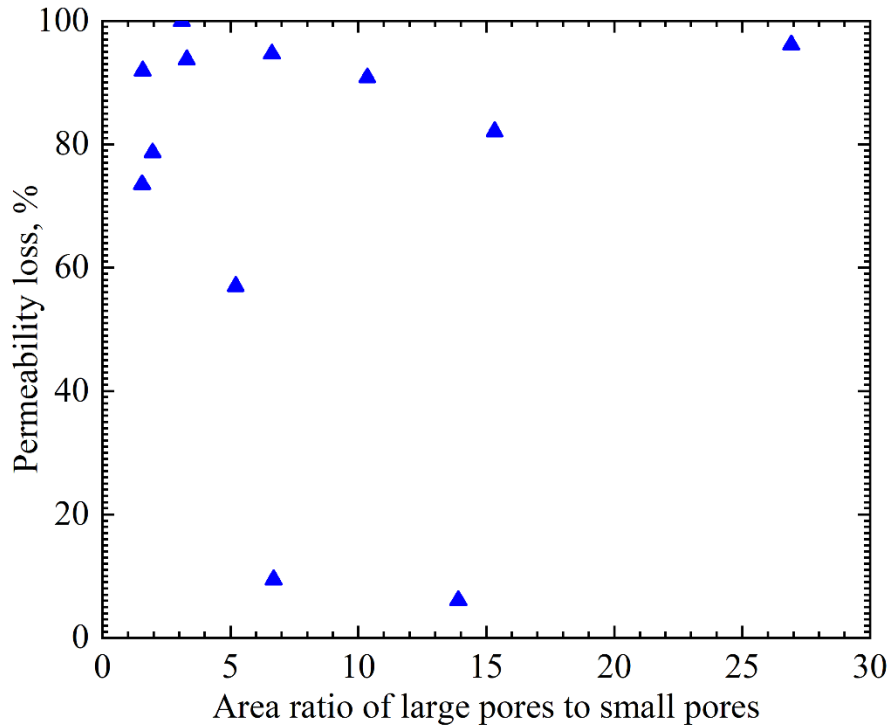
Core No.	Porosity, %	Permeability, mD	Final permeability loss, %	Total stabilization time, h	Area ratio of large pores to small pores	Slope of the cumulative stabilization time curve
1	4.1	0.0236	96.13%	26	26.741	10.377
2	8.8	0.0754	56.98%	23	13.847	10.662
3	9.7	0.0843	90.81%	26	11.497	9.928
4	17.8	129.0900	6.07%	9	55.627	4.230
5	16.0	10.9700	9.42%	6	89.858	2.732
6	6.5	0.0524	82.05%	14	33.229	6.197
7	2.7	0.0396	94.66%	17	25.645	7.931
8	14.0	0.4786	93.71%	148	3.293	57.360
9	12.5	0.4723	91.92%	139	1.574	55.834
10	16.3	0.9310	78.64%	166	1.965	76.812
11	15.7	0.9889	73.48%	144	1.549	64.788
12	12.7	0.4081	99.95%	75	3.103	36.600



(a)



(b)



(c)

Figure 7 Plots of permeability loss versus: (a) permeability; (b) porosity; (c) area ratio of large pores to small pores.

3.4. Dependence of Cumulative Stabilization Time on Area Ratio of Large Pores to Small Pores

Based on the results shown in Table 5, an attempt is made to explore the possible dependence of the slope of the cumulative stabilization time curve on the core properties.

Figure 8 shows the plots of the slope of the cumulative stabilization time curve versus permeability, porosity, and area ratio of large pores to small pores. As seen from Figure 8, the slope of the cumulative stabilization time curve does not show a correlation with either permeability or porosity of the core samples (See Figures 8a and 8b). Instead, it shows a strong correlation with the area ratios of the core samples (See Figures 8c). As Figure 8(c)

shows, the slope of cumulative stabilization time and confining pressure strongly correlates ($R^2=0.86$) with the area ratio of large pores to small pores. The relationship between the slope of the cumulative stabilization time curve and the area ratio can be established by regression:

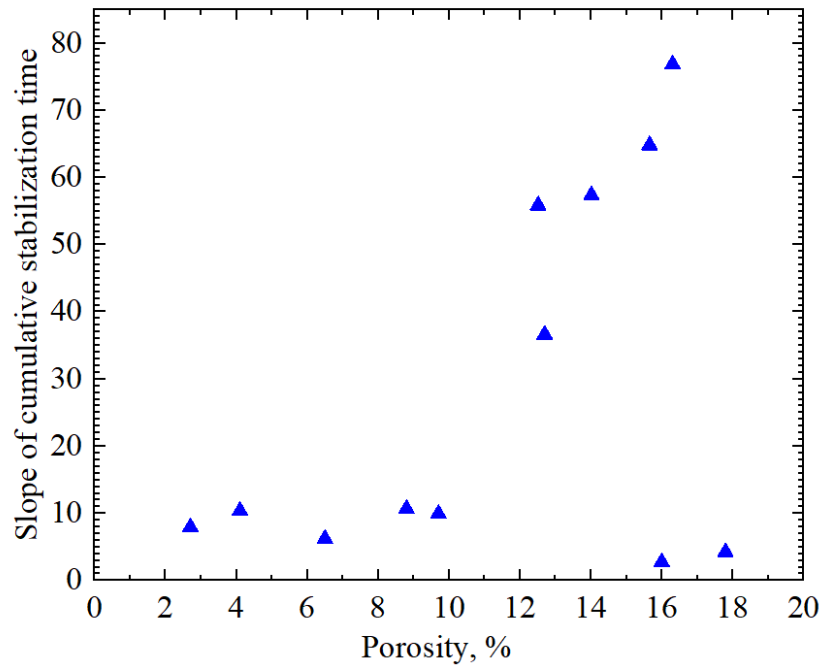
$$A = 3.9760 + 117.4976 * 0.6858^R \quad (3)$$

where R is the area ratio of large pores to small pores. Equation 3 generates a large correlation coefficient of $R^2=0.86$. Equation 3 indicates that the slope of the cumulative stabilization time curve is inversely proportional to the pore-throat area ratio. Once the area ratio is determined from a MIP test, it can be then used to predict the slope of the cumulative stabilization time curve. Thereafter, Equation 2 can be applied to predict how much stabilization time is needed by a given core sample at a given confining pressure. Appendix A gives an example calculation which explains how to predict the stabilization time during stress-sensitivity tests using Equations 2 and 3.

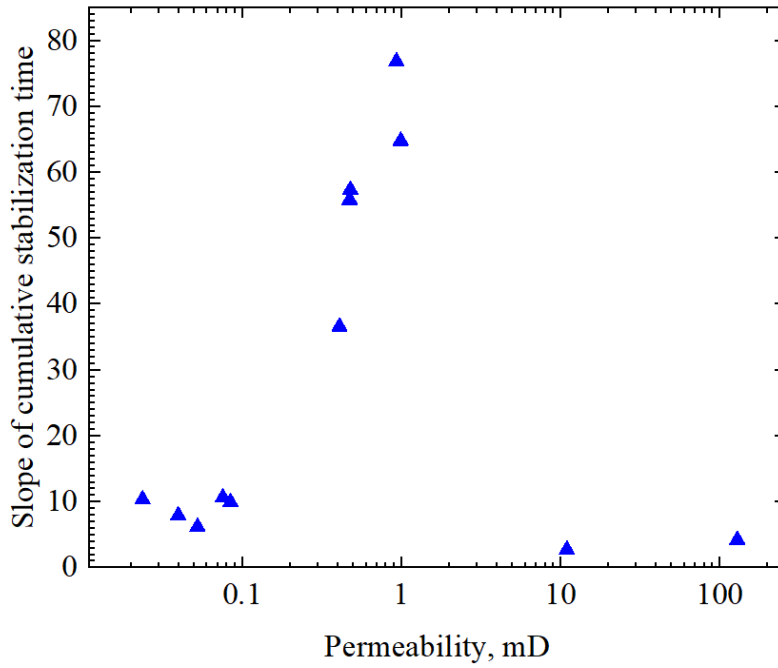
The above finding validates our hypothesis that that the delayed stress sensitivity phenomenon is dependent on the pore-structure properties of a given porous medium. The pore-structure property is found to be the area ratio of large pores to small pores in this study. Physically, a core with a smaller area ratio has more smaller pores, resulting in a steadier structure. Such a steadier structure makes the core deform more slowly, yielding longer stabilization durations.

We believe that the above finding should be valid for other core samples that are not tested in this study, since the 12 core samples cover a large spectrum of physical properties. Nonetheless, the universality of Equation 3 should be further tested with more

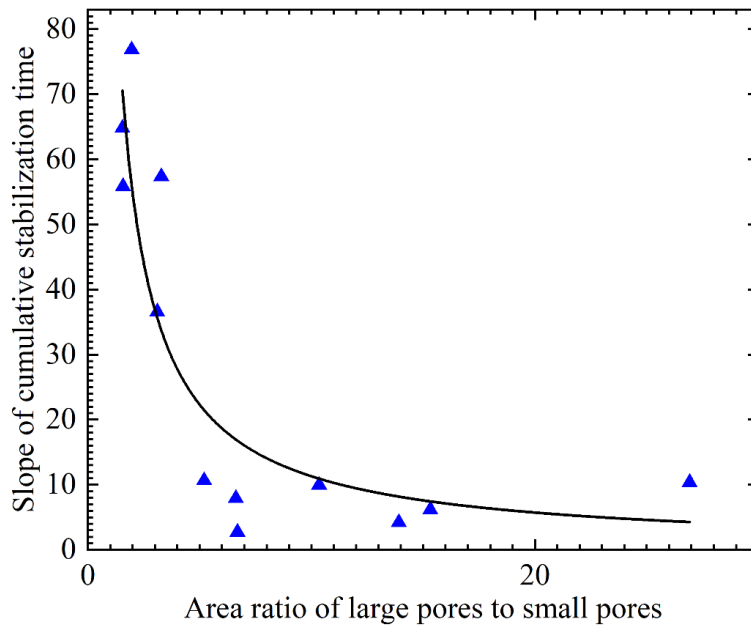
experimental works using more core samples. As such, we should be cautious when applying Equations 2 and 3 to other core samples.



(a)



(b)



(c)

Figure 8 Plots of the slope of the cumulative stabilization time curve versus: (a) porosity; (b) permeability; (c) area ratio of large pores and small pores.

References

Liu, K, Yin, D.Y., Sun, Y.H. The mathematical model of stress sensitivities on tight reservoirs of different sedimentary rocks and its application. *J. Pet. Sci. Eng.* 2020, **193**: 107372.

CHAPTER 4 CONCLUSIONS AND RECOMMENDATIONS

4.1. Conclusions

In this research, we conduct experiments on 12 core samples to determine the stabilization time during stress-sensitivity tests. We try to understand which parameters control the durations of the stabilization time exhibited by different core samples. MIP tests are conducted to measure the pore size distributions of the 12 core samples. Tri-axial stress-sensitivity tests are also conducted on these 12 core samples. The following conclusions can be obtained based on the experimental results and their interpretation:

- An empirical method is developed to split the pores in a given core sample into large pores and small pores based on the pore size distribution charts. We further calculate the area ratio of large pores to small pores.
- We monitor the variation of permeability versus time during each tri-axial stress-sensitivity test. We observe in the stress-sensitivity tests that it takes some time for the permeability to reach a constant value when the confining pressure rises to a given level. The time needed to reach a constant permeability value is defined as the stabilization time during a tri-axial stress-sensitivity test.
- When analyzing the stress-sensitivity test results, the cumulative stabilization time is recorded as a function of the confining pressure. The cumulative stabilization time (T) is found to linearly correlate with the logarithm function of the confining pressure ($\ln P$). The slope of the linear relationship between T and $\ln P$ shows a strong correlation with the area ratio of large pores to the small pores.

- The experimental and analytical results indicate that a core sample with a larger area ratio of large pores to small pores has a shorter stabilization time, while a core sample with a smaller area ratio of large pores to small pores has a longer stabilization time. This agrees well with the physical understanding that the core sample with a smaller area ratio of large pores to smaller pores tends to have a steadier structure and deform more slowly than the one with a larger area ratio of large pores to smaller pores.

4.2. Recommendations

In this research, MIP tests and tri-axial stress sensitivity tests are conducted on a total of 12 sandstone core samples. The relationship between the slope of the cumulative stabilization time and the area ratio of large pores to small pores shows a high correlation coefficient of $R^2=0.86$. Using this relationship, we can predict how much time is needed to reach the stabilization time during a stress-sensitivity test. Although the 12 core samples cover a large spectrum of physical properties and we believe that the correlation should be valid for other sandstone core samples, the established correlation between the cumulative stabilization time and the area ratio of large pores to small pores should be further validated by additional stress-sensitivity tests conducted on more core samples (for example, carbonate cores).

The empirical method developed in this study relies on MIP tests to estimate the area ratio of large pores to small pores. In future work, other methods such as gas adsorption and NMR techniques should be considered to provide a more comprehensive picture of the pore structures of a given core sample. In addition, in order to better simulate the actual

stress conditions in the reservoir, the stress-sensitivity tests should be conducted under higher temperature and pressure conditions that are encountered by typical tight reservoirs.

BIBLIOGRAPHY

- Cao, N., Lei, G. Stress sensitivity of tight reservoirs during pressure loading and unloading process. *J. Petrol. Explor. Dev.* 2019, **46** (1): 132-138.
- Fatt, I., Davis, D.H. Reduction in permeability with overburden pressure. *J. Pet. Tech.* 1952, **4** (12): 16.
- Gangi, A.F. Hertz theory applied to the porosity-pressure, permeability-pressure and failure strength-porosity variations of porous rocks. ARMA-76-0119, 1976.
- Ge, J., Jerath, S., Ghassemi, A., Ling, K. Sensitivity study on the poroelastic and thermoelastic effects on the stress reversal nearby an existing hydraulic fracture. ARMA-2018-287, 2018.
- Heidari Sureshjani, M., Clarkson, C.R. An analytical model for analyzing and forecasting production from multifractured horizontal wells with complex branched fracture geometry. *SPE Res Eval & Eng.* 2015, **18** (3): 356-374.
- Iscan, A.G., Kok, M.V., Bagc, A.S. Estimation of permeability and rock mechanical properties of limestone reservoir rocks under stress conditions by strain gauge. *J. Pet. Sci. Eng.* 2006, **53** (1): 13-24.
- Jiang, L., Liu, J., Liu, T., Yang, D. Semi-analytical modeling of transient pressure behaviour for a fractured vertical well with hydraulic/natural fracture networks by considering stress-sensitive effect. *J. Nat. Gas Sci. Eng.* 2020. **82**: 103477.

- Jones, F.O. A laboratory study of effects of confining pressure on fracture flow and storage capacity in carbonate rocks. *J. Pet. Tech.* 1975, **27** (1): 21-27.
- Jose, G. Numerical simulation of coupled fluid-flow/geomechanical behavior of tight gas reservoirs with stress sensitive permeability. SPE-39055, 1997.
- Li, Y.D., Dong, P.C. Stress sensitivity analysis of permeability and threshold pressure gradient in low-permeability reservoirs. *Pet. Geol. Recovery Effi.* 2016, **23** (6): 57-63 (In Chinese).
- Liu, J., Jiang, L., Liu, T., Yang, D. Modeling tracer flowback behaviour for a fractured vertical well in a tight formation by coupling fluid flow and geomechanical dynamics. *J. Nat. Gas Sci. Eng.* 2020, **84**: 103656.
- Liu, K, Yin, D.Y., Sun, Y.H. The mathematical model of stress sensitivities on tight reservoirs of different sedimentary rocks and its application. *J. Pet. Sci. Eng.* 2020, **193**: 107372.
- Liu, R.J., Liu, H.Q. Study of stress sensitivity and its influence on oil development in low permeability reservoir. *J. Rock. Mech. Eng.* 2011, **30** (S1): 2697 (In Chinese).
- Mckee, C.R., Bumb, A.C, Koenig, R.A. Stress dependent permeability and porosity of coal and other geologic formations. *SPE Form. Eval.* 1988, **3** (1): 81-91.
- Nie, X.R, Wang, C.L, Liu, J. Experimental study on stress sensitivity for tight reservoirs based on time scale. *J. Unconv. Oil Gas* 2016, **3** (4): 22-24 (In Chinese).

- Wei, M., Duan, Y., Dong, M., Fang, Q., Dejam, M. Transient production decline behavior analysis for a multi-fractured horizontal well with discrete fracture networks in shale gas reservoirs. *J. Porous. Media.* 2019, **22** (3): 343-361.
- Yang, Y.F., Zhang, W.J., Gao, Y., Wan, Y.J., Su, Y.H., An, S.Y., Sun, H., Zhang, L., Zhao, J., Liu, L., Liu, P., Liu, Z., Li, A., Yao, J. Influence of stress sensitivity on microscopic pore structure and fluid flow in porous media. *J. Nat. Gas Sci. Eng.* 2016, **36**: 20-31.
- Yin, S.X., Wang, S.X. Effect and mechanism of stresses on rock permeability at different scales. *SCI China Ser. D.* 2006, **36** (5): 472-480.
- Zhang, W.T., Wang, Q., Ning, Z.H.F., Zhang, R., Huang, L., Cheng, Z.H.L. Relationship between the stress sensitivity and pore structure of shale. *J. Nat. Gas. Sci. Eng.* 2018, **59**: 440-451.
- Zhang, Y.H., Yang, D.Y. Evaluation of transient pressure responses of a hydraulically fractured horizontal well in a tight reservoir with an arbitrary shape by considering stress-sensitive effect. *J. Pet. Sci. Eng.* 2021, **202**: 108518.
- Zhang, Y.H., Yang, D.Y. Modeling transient pressure behaviour of a multi-fractured horizontal well in a reservoir with an arbitrary boundary and different fracture networks by considering stress-sensitive effect. *J. Hydrol.* 2021, **600**: 126552.
- Zhang, Z., He, S., Liu, G., Guo, X., Mo, S. Pressure buildup behavior of vertically fractured wells with stress-sensitive conductivity. *J. Pet. Sci. Eng.* 2014, **122**: 48-55.

Zhu, B. Standard method for evaluating stress-sensitivity flow tests. Petroleum Industry Standard of China. 2002, SY/T 5358 (In Chinese).

APPENDIX A: AN EXAMPLE CALCULATION SHOWING HOW TO PREDICT STABILIZATION TIME DURING STRESS-SENSITIVITY TESTS USING THE ESTABLISHED EMPIRICAL CORRELATIONS

We assume that a tight sandstone core sample is extracted from a field and stress sensitivity tests need to be conducted on this core sample. Below we show the detailed calculation procedure that uses the established empirical correlations to predict the stabilization time when the confining pressure is changed from: 1) 5 MPa to 10 MPa; 2) 5 MPa to 30 MPa.

1) Step 1. First, MIP test needs to be conducted to obtain the pore geometry parameters, including pore-throat area ratio. Let us assume that the measured pore-throat area ratio is 20.

2) Step 2. Calculate the slope of the cumulative stabilization time as per Equation 2:

$$\begin{aligned} A &= 3.9760 + 117.4976 * 0.6858^R = 3.9759 + 117.4976 * 0.6858^{20} \\ &= 4.0382 \end{aligned}$$

3) Step 3. Express the logarithmic correlation between the cumulative stabilization time and the confining pressure as follows:

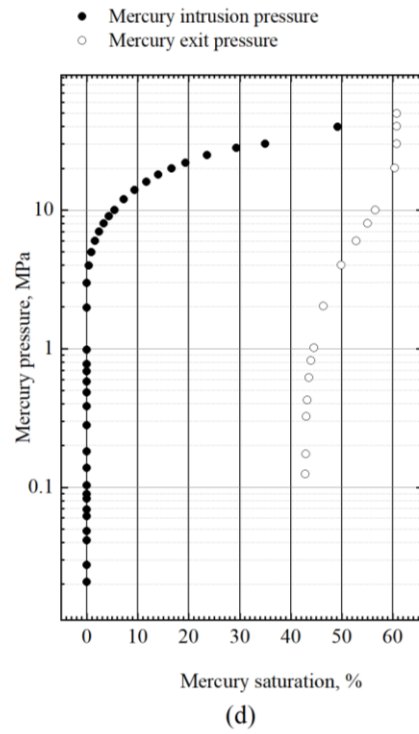
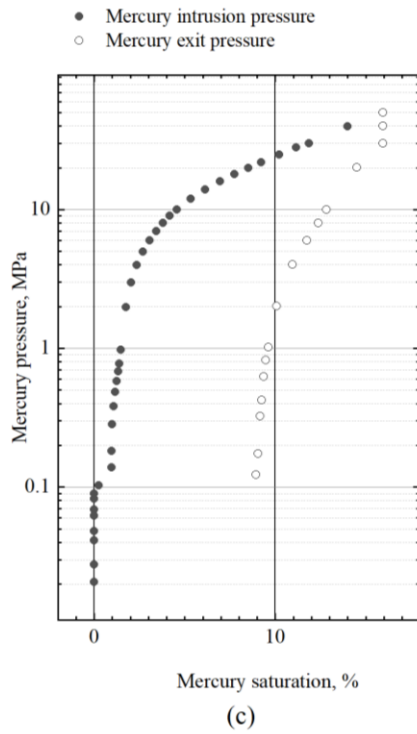
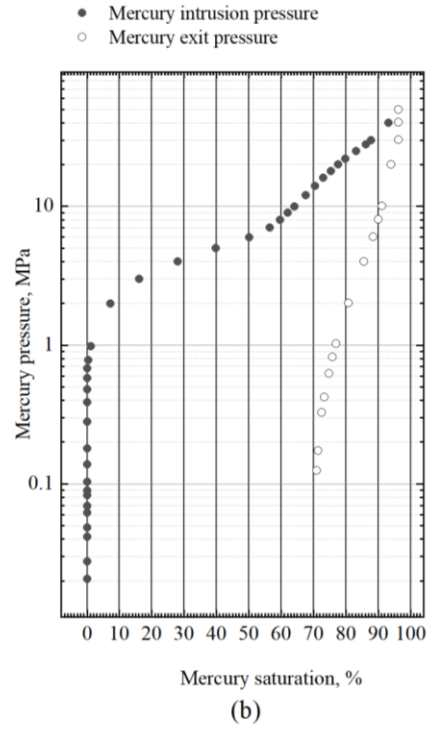
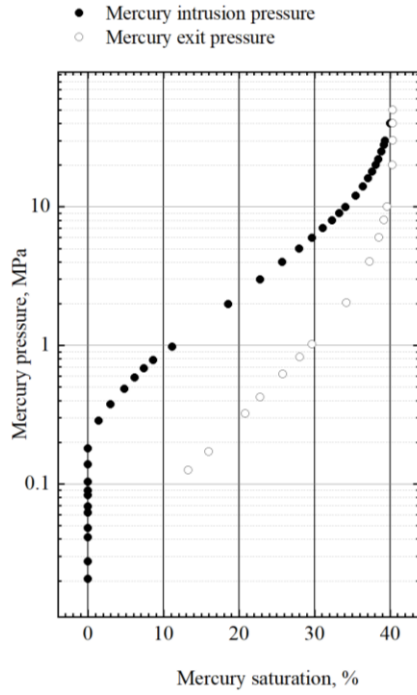
$$T = A \ln P + B = 4.0382 \ln P + B$$

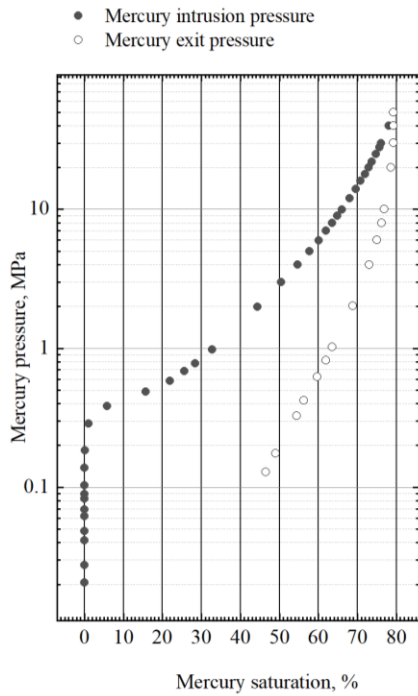
4) Step 4. Calculate the stabilization time required during the stress-sensitivity tests when the confining pressure rises from 5 MPa to 10 MPa:

$$\begin{aligned} \Delta T_1 &= T(10) - T(5) = 4.0382 \ln 10 + B - (4.0382 \ln 5 + B) \\ &= 4.0382 \ln 10 - 4.0382 \ln 5 = 2.80 \text{ hours} \end{aligned}$$

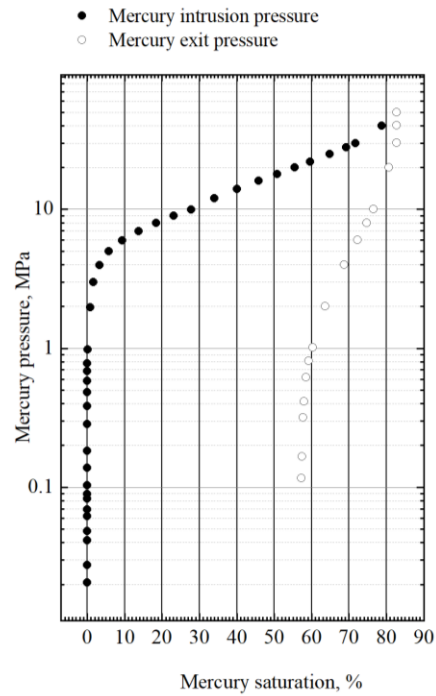
By carrying out the same calculation for the case where the confining pressure rises from 5 MPa to 30 MPa, we can obtain $\Delta T_2 = 7.24 \text{ hours}$.

APPENDIX B: DETAILED MIP TEST RESULTS

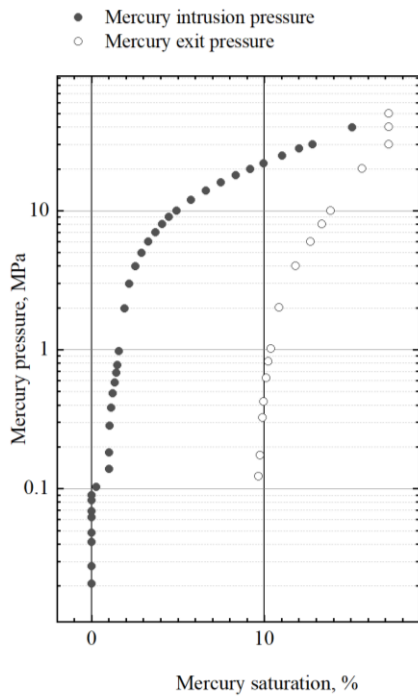




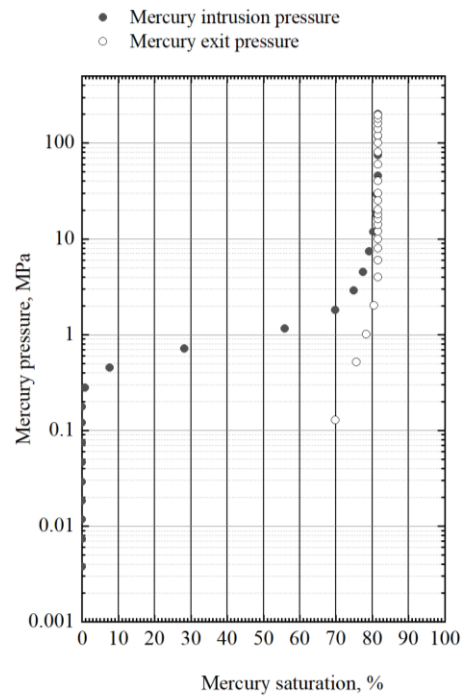
(e)



(f)



(g)



(h)

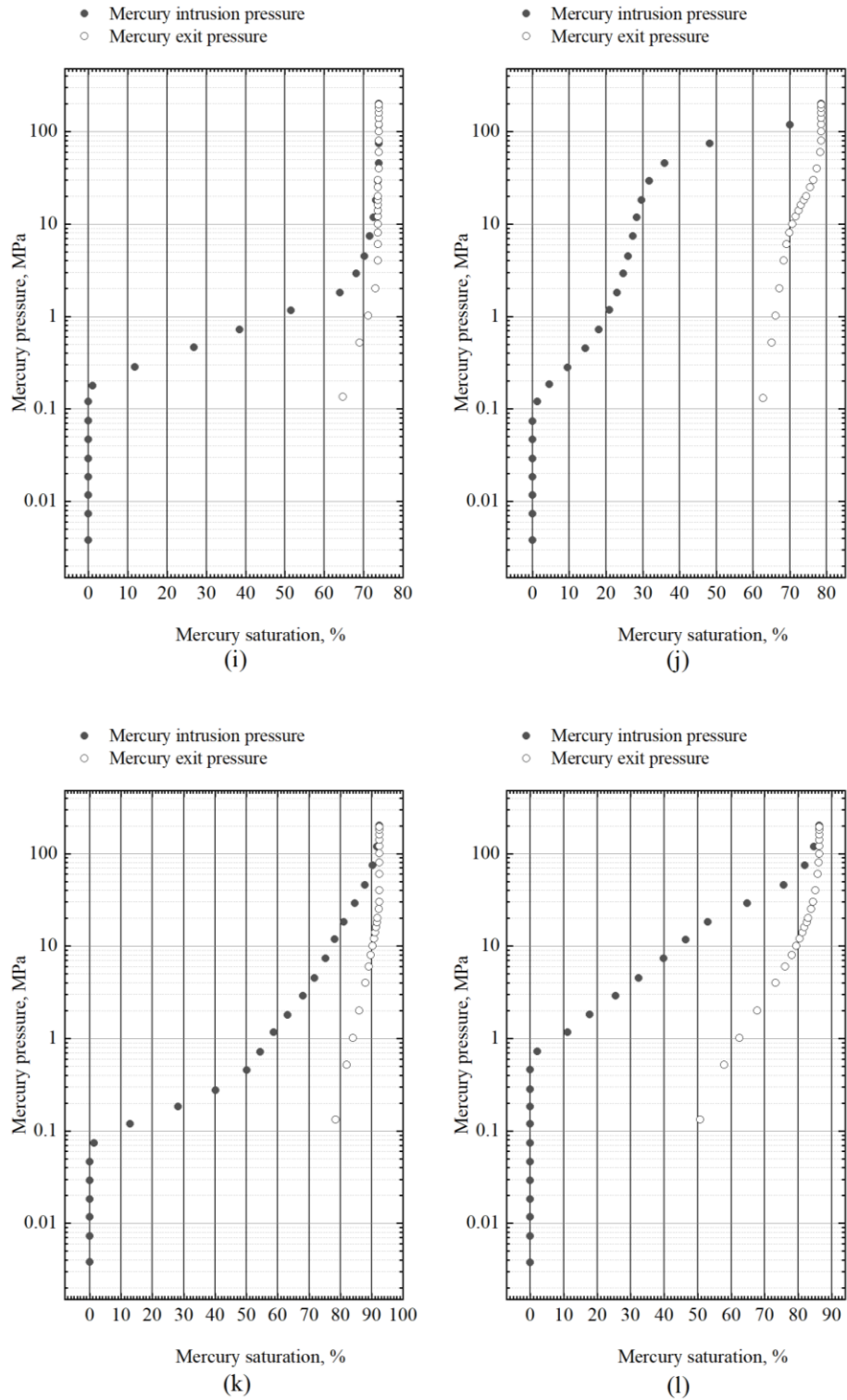


Figure 9 MIP test results for: (a) core 1, (b) core 2, (c) core 3, (d) core 4, (e) core 5, (f) core 6, (g) core 7, (h) core 8, (i) core 9, (j) core 10, (k) core 11, and (l) core 12.

Table 6 Results of the MIP test conducted on the core sample 1

No.	Pore size, μm	Mercury saturation, %	Permeability contribution, %	Frequency, %	Pore area, μm^2
1	30.6463	0.0000	0.0000	0.0000	0.0000
2	22.1531	0.0000	0.0000	0.0000	0.0000
3	16.0136	0.0000	0.0000	0.0000	0.0000
4	11.5757	0.0000	0.0000	0.0000	0.0000
5	8.3676	1.4600	44.9975	0.2981	20.8714
6	6.0486	1.7600	51.4208	0.6519	23.8508
7	4.3723	2.0300	0.2687	0.0065	0.1246
8	3.1606	2.3500	0.4750	0.0221	0.2203
9	2.2847	2.6900	1.0326	0.0918	0.4790
10	1.6515	3.0500	0.7629	0.1297	0.3539
11	1.1938	3.4300	0.4854	0.1580	0.2251
12	0.8630	3.7900	0.1898	0.1182	0.0880
13	0.6238	4.1600	0.1159	0.1381	0.0538
14	0.4509	4.5600	0.0606	0.1381	0.0281
15	0.3260	5.3400	0.0479	0.2091	0.0222
16	0.2356	6.1300	0.0375	0.3129	0.0174
17	0.1703	6.9600	0.0299	0.4782	0.0139
18	0.1231	7.7500	0.0238	0.7269	0.0110
19	0.0890	8.5100	0.0175	1.0262	0.0081
20	0.0643	9.2300	0.0133	1.4899	0.0062
21	0.0465	10.2100	0.0098	2.0928	0.0045
22	0.0336	11.1400	0.0060	2.4755	0.0028
23	0.0243	11.8500	0.0034	2.6778	0.0016
24	0.0176	14.0000	0.0018	2.7182	0.0008

Table 7 Results of the MIP test conducted on the core sample 2

No.	Pore size, μm	Mercury saturation, %	Permeability contribution, %	Frequency, %	Pore area, μm^2
1	30.6103	0.0000	0.0000	0.0000	0.0000
2	22.1279	0.0000	0.0000	0.0000	0.0000
3	15.9961	0.0000	0.0000	0.0000	0.0000
4	11.5634	0.0000	0.0000	0.0000	0.0000
5	8.3591	0.0000	0.0000	0.0000	0.0000
6	6.0427	0.0000	0.0000	0.0000	0.0000
7	4.3682	0.0000	0.0000	0.0000	0.0000
8	3.1578	0.0000	0.0000	0.0000	0.0000
9	2.2827	0.0000	0.0000	0.0000	0.0000
10	1.6502	0.0000	0.0000	0.0000	0.0000
11	1.1929	0.3600	5.7006	0.2028	0.2885
12	0.8623	7.3000	18.2250	1.2405	0.9224
13	0.6234	16.1600	21.8759	2.8493	1.1072
14	0.4506	28.1000	11.4318	2.8493	0.5786
15	0.3258	39.8800	14.2289	6.7866	0.7202
16	0.2355	50.0800	12.4275	11.3427	0.6290
17	0.1702	59.7000	9.3845	16.3907	0.4750
18	0.1231	64.1700	4.5817	15.3133	0.2319
19	0.0890	67.6700	1.0820	6.9201	0.0548
20	0.0643	75.3800	0.5032	6.1590	0.0255
21	0.0465	79.8400	0.2702	6.3282	0.0137
22	0.0336	83.2100	0.1774	7.9530	0.0090
23	0.0243	86.1600	0.0818	7.0116	0.0041
24	0.0176	87.7600	0.0296	4.8530	0.0015

Table 8 Results of the MIP test conducted on the core sample 3

No.	Pore size, μm	Mercury saturation, %	Permeability contribution, %	Frequency, %	Pore area, μm^2
1	1.1671	0.0000	0.0000	0.0000	0.0000
2	0.9691	0.0000	0.0000	0.0000	0.0000
3	0.8047	0.0000	0.0000	0.0000	0.0000
4	0.6683	0.0000	0.0000	0.0000	0.0000
5	0.5549	0.0000	0.0000	0.0000	0.0000
6	0.4608	0.0000	0.0000	0.0000	0.0000
7	0.3826	0.0000	0.0000	0.0000	0.0000
8	0.3177	0.0000	0.0000	0.0000	0.0000
9	0.2638	28.0000	2.2429	0.0440	0.0031
10	0.2191	29.0000	9.6881	0.2759	0.0132
11	0.1819	30.0000	9.1964	0.3797	0.0126
12	0.1511	31.0000	8.8775	0.5316	0.0121
13	0.1255	32.0000	9.0025	0.7818	0.0123
14	0.1042	33.0000	9.1509	1.1525	0.0125
15	0.0865	34.0000	8.7354	1.5955	0.0119
16	0.0718	35.0000	7.2347	1.9163	0.0099
17	0.0597	36.0000	6.0518	2.3247	0.0083
18	0.0495	37.0000	5.6487	3.1468	0.0077
19	0.0411	38.0000	5.1018	4.1217	0.0070
20	0.0342	39.0000	4.8112	5.6369	0.0066
21	0.0284	40.0000	5.4449	9.2515	0.0074
22	0.0236	41.0000	4.3608	10.7454	0.0060
23	0.0196	42.0000	2.5909	9.2586	0.0035
24	0.0162	43.0000	1.8615	9.6469	0.0025

Table 9 Results of the MIP test conducted on the core sample 4

No.	Pore size, μm	Mercury saturation, %	Permeability contribution, %	Frequency, %	Pore area, μm^2
1	30.6529	0.0000	0.0000	0.0000	0.0000
2	22.1572	0.0000	0.0000	0.0000	0.0000
3	16.0161	0.0000	0.0000	0.0000	0.0000
4	11.5771	0.0000	0.0000	0.0000	0.0000
5	8.3684	0.0000	0.0000	0.0000	0.0000
6	6.0491	0.0000	0.0000	0.0000	0.0000
7	4.3725	1.4300	15.0372	0.3222	6.1608
8	3.1606	4.7800	24.6204	1.0098	10.0871
9	2.2846	7.4000	22.5512	1.7701	9.2393
10	1.6514	11.1100	15.8046	2.3743	6.4752
11	1.1937	18.5700	9.0629	2.6057	3.7131
12	0.8629	22.7900	6.2177	3.4214	2.5474
13	0.6237	25.7500	3.2571	3.4303	1.3345
14	0.4509	27.9400	1.7019	3.4303	0.6973
15	0.3259	29.6800	0.8707	3.3589	0.3567
16	0.2356	31.0900	0.4499	3.3213	0.1843
17	0.1703	33.2800	0.2260	3.1933	0.0926
18	0.1231	35.4600	0.1117	3.0198	0.0458
19	0.0890	36.4000	0.0528	2.7331	0.0216
20	0.0643	37.1000	0.0227	2.2476	0.0093
21	0.0465	38.1000	0.0085	1.6171	0.0035
22	0.0336	38.8900	0.0032	1.1610	0.0013
23	0.0243	39.2200	0.0011	0.7880	0.0005
24	0.0176	40.0400	0.0004	0.5956	0.0002

Table 10 Results of the MIP test conducted on the core sample 5

No.	Pore size, μm	Mercury saturation, %	Permeability contribution, %	Frequency, %	Pore area, μm^2
1	30.6537	0.0000	0.0000	0.0000	0.0000
2	22.1585	0.0000	0.0000	0.0000	0.0000
3	16.0176	0.0000	0.0000	0.0000	0.0000
4	11.5785	0.0000	0.0000	0.0000	0.0000
5	8.3697	0.0000	0.0000	0.0000	0.0000
6	6.0502	5.8000	0.8471	0.0218	0.7976
7	4.3734	15.7500	5.8775	0.2893	5.5342
8	3.1614	21.9600	7.3614	0.6935	6.9315
9	2.2853	25.6900	26.4276	4.7649	24.8842
10	1.6519	28.4100	37.2094	12.8390	35.0363
11	1.1941	32.7800	12.9366	8.5426	12.1811
12	0.8632	44.3200	4.8927	6.1830	4.6069
13	0.6240	50.5000	2.2003	5.3213	2.0718
14	0.4510	57.6900	1.1497	5.3213	1.0826
15	0.3260	60.0600	0.5567	4.9308	0.5242
16	0.2357	64.8600	0.2803	4.7510	0.2639
17	0.1704	66.0300	0.1368	4.4388	0.1288
18	0.1232	69.5500	0.0653	4.0542	0.0615
19	0.0890	72.8800	0.0313	3.7140	0.0294
20	0.0644	73.6900	0.0150	3.4091	0.0141
21	0.0465	74.7600	0.0071	3.0791	0.0067
22	0.0336	75.6300	0.0033	2.7349	0.0031
23	0.0243	76.0300	0.0014	2.2296	0.0013
24	0.0176	78.0200	0.0006	1.9218	0.0006

Table 11 Results of the MIP test conducted on the core sample 6

No.	Pore size, μm	Mercury saturation, %	Permeability contribution, %	Frequency, %	Pore area, μm^2
1	30.6463	0.0000	0.0000	0.0000	0.0000
2	22.1533	0.0000	0.0000	0.0000	0.0000
3	16.0139	0.0000	0.0000	0.0000	0.0000
4	11.5760	0.0000	0.0000	0.0000	0.0000
5	8.3679	0.0000	0.0000	0.0000	0.0000
6	6.0489	0.0000	0.0000	0.0000	0.0000
7	4.3726	0.0000	0.0000	0.0000	0.0000
8	3.1608	0.0000	0.0000	0.0000	0.0000
9	2.2849	0.0000	0.0000	0.0000	0.0000
10	1.6517	0.0000	0.0000	0.0000	0.0000
11	1.1939	0.0000	0.0000	0.0000	0.0000
12	0.8631	0.7800	11.6707	0.1358	0.1011
13	0.6239	5.8300	14.0849	0.3135	0.1220
14	0.4510	13.6900	7.3599	0.3135	0.0638
15	0.3260	27.8100	8.3582	0.6814	0.0724
16	0.2357	34.0200	9.2228	1.4389	0.0799
17	0.1703	40.0900	11.9298	3.5620	0.1034
18	0.1231	45.7800	13.8342	7.9048	0.1199
19	0.0890	50.8500	11.7354	12.8327	0.1017
20	0.0643	55.5000	5.6778	11.8819	0.0492
21	0.0465	59.5900	3.4615	13.8627	0.0300
22	0.0336	64.8000	1.7682	13.5519	0.0153
23	0.0243	69.2000	0.6674	9.7889	0.0058
24	0.0176	78.7700	0.2291	6.4319	0.0020

Table 12 Results of the MIP test conducted on the core sample 7

No.	Pore size, μm	Mercury saturation, %	Permeability contribution, %	Frequency, %	Pore area, μm^2
1	6.3257	0.2800	86.8793	0.6516	26.0749
2	4.8891	1.1500	7.0372	0.0884	2.1121
3	3.7789	1.3500	0.8774	0.0184	0.2633
4	2.9207	1.4900	0.7791	0.0274	0.2338
5	2.2574	1.5800	1.3009	0.0766	0.3904
6	1.7448	1.9000	0.9824	0.0968	0.2948
7	1.3486	2.1900	0.9173	0.1514	0.2753
8	1.0423	2.5400	0.4179	0.1155	0.1254
9	0.8056	2.9000	0.2270	0.1050	0.0681
10	0.6227	3.2800	0.1511	0.1169	0.0453
11	0.4813	3.7000	0.0902	0.1169	0.0271
12	0.3720	4.0900	0.0698	0.1513	0.0209
13	0.2875	4.4900	0.0501	0.1818	0.0150
14	0.2222	4.9200	0.0500	0.3040	0.0150
15	0.1717	5.7600	0.0388	0.3943	0.0116
16	0.1327	6.6100	0.0332	0.5654	0.0100
17	0.1026	7.5000	0.0261	0.7449	0.0078
18	0.0793	8.3600	0.0214	1.0231	0.0064
19	0.0613	9.1800	0.0164	1.3116	0.0049
20	0.0474	9.9600	0.0132	1.7663	0.0040
21	0.0366	11.0200	0.0092	2.0647	0.0028
22	0.0283	12.0100	0.0064	2.3814	0.0019
23	0.0219	12.7800	0.0033	2.0867	0.0010
24	0.0169	15.1000	0.0023	2.3895	0.0007

Table 13 Results of the MIP test conducted on the core sample 9

No.	Pore size, μm	Mercury saturation, %	Permeability contribution, %	Frequency, %	Pore area, μm^2
1	193.2208	0.0000	0.0000	0.0000	0.0000
2	100.3429	0.0000	0.0000	0.0000	0.0000
3	62.7645	0.0000	0.0000	0.0000	0.0000
4	40.1378	0.0000	0.0000	0.0000	0.0000
5	25.2686	0.0000	0.0000	0.0000	0.0000
6	15.7859	0.0000	0.0000	0.0000	0.0000
7	9.9393	0.0000	0.0000	0.0000	0.0000
8	6.1351	0.0000	0.0000	0.0000	0.0000
9	4.1075	1.0674	11.1617	1.0674	18.0088
10	2.6007	11.8528	48.9005	10.7854	72.9506
11	1.5941	26.8710	26.8074	15.0182	38.1657
12	1.0214	38.4285	7.9474	11.5574	12.0584
13	0.6294	51.4995	3.6093	13.0710	5.1776
14	0.4060	63.9538	1.3401	12.4544	2.0527
15	0.2527	68.1526	0.1842	4.1988	0.2682
16	0.1632	70.2601	0.0366	2.1074	0.0561
17	0.0996	71.5855	0.0093	1.3254	0.0131
18	0.0624	72.5460	0.0025	0.9605	0.0037
19	0.0405	73.1767	0.0007	0.6307	0.0010
20	0.0252	73.6280	0.0002	0.4513	0.0003
21	0.0161	73.8559	0.0000	0.2279	0.0001
22	0.0099	73.9069	0.0000	0.0510	0.0000
23	0.0062	73.9069	0.0000	0.0000	0.0000
24	0.0037	73.9069	0.0000	0.0000	0.0000

Table 14 Results of the MIP test conducted on the core sample 10

No.	Pore size, μm	Mercury saturation, %	Permeability contribution, %	Frequency, %	Pore area, μm^2
1	194.6135	0.0000	0.0000	0.0000	0.0000
2	100.7217	0.0000	0.0000	0.0000	0.0000
3	62.8351	0.0000	0.0000	0.0000	0.0000
4	40.2179	0.0000	0.0000	0.0000	0.0000
5	25.2829	0.0000	0.0000	0.0000	0.0000
6	15.8125	0.0000	0.0000	0.0000	0.0000
7	9.9463	0.0000	0.0000	0.0000	0.0000
8	6.1403	1.2853	32.9374	1.2853	48.4614
9	4.0018	4.6341	33.7383	3.3488	53.6283
10	2.6266	9.5093	20.9503	4.8751	33.6341
11	1.6187	14.4137	8.7563	4.9045	12.8510
12	1.0236	18.0568	2.5062	3.6430	3.8170
13	0.6292	20.9770	0.7907	2.9203	1.1560
14	0.4068	22.9555	0.2083	1.9784	0.3274
15	0.2533	24.6626	0.0735	1.7071	0.1095
16	0.1638	26.0113	0.0230	1.3487	0.0362
17	0.0996	27.2735	0.0087	1.2622	0.0125
18	0.0624	28.4203	0.0030	1.1468	0.0045
19	0.0405	29.6755	0.0013	1.2551	0.0021
20	0.0252	31.7336	0.0009	2.0582	0.0013
21	0.0161	35.9396	0.0007	4.2060	0.0011
22	0.0099	48.1661	0.0008	12.2264	0.0012
23	0.0062	69.9499	0.0006	21.7838	0.0008
24	0.0037	78.4963	0.0001	8.5465	0.0001

Table 15 Results of the MIP test conducted on the core sample 11

No.	Pore size, μm	Mercury saturation, %	Permeability contribution, %	Frequency, %	Pore area, μm^2
1	193.6052	0.0000	0.0000	0.0000	0.0000
2	100.7232	0.0000	0.0000	0.0000	0.0000
3	62.9117	0.0000	0.0000	0.0000	0.0000
4	40.1849	0.0000	0.0000	0.0000	0.0000
5	25.2978	0.0000	0.0000	0.0000	0.0000
6	15.7996	0.0000	0.0000	0.0000	0.0000
7	9.9502	1.3184	14.0130	1.3184	130.5292
8	6.1398	12.8699	46.7483	11.5515	435.4526
9	4.0016	28.2689	26.4716	15.3990	246.5789
10	2.6813	40.1846	9.1966	11.9157	85.6645
11	1.6085	50.1900	2.7792	10.0054	25.8876
12	1.0238	54.4177	0.4757	4.2277	4.4311
13	0.6314	58.7922	0.1872	4.3745	1.7441
14	0.4080	63.1758	0.0783	4.3836	0.7297
15	0.2529	68.0542	0.0335	4.8784	0.3121
16	0.1637	71.7527	0.0106	3.6985	0.0991
17	0.0996	75.2607	0.0037	3.5080	0.0348
18	0.0624	78.2146	0.0012	2.9539	0.0115
19	0.0405	81.1757	0.0005	2.9611	0.0048
20	0.0252	84.6362	0.0002	3.4605	0.0022
21	0.0161	87.8007	0.0001	3.1646	0.0008
22	0.0099	90.3560	0.0000	2.5553	0.0002
23	0.0062	91.7295	0.0000	1.3735	0.0001
24	0.0037	92.5189	0.0000	0.7894	0.0000

Table 16 Results of the MIP test conducted on the core sample 12

No.	Pore size, μm	Mercury saturation, %	Permeability contribution, %	Frequency, %	Pore area, μm^2
1	194.6135	0.0000	0.0000	0.0000	0.0000
2	100.7217	0.0000	0.0000	0.0000	0.0000
3	62.8351	0.0000	0.0000	0.0000	0.0000
4	40.2179	0.0000	0.0000	0.0000	0.0000
5	25.2829	0.0000	0.0000	0.0000	0.0000
6	15.8125	0.0000	0.0000	0.0000	0.0000
7	9.9463	0.0000	0.0000	0.0000	0.0000
8	6.1403	0.0000	0.0000	0.0000	0.0000
9	4.0018	0.0000	0.0000	0.0000	0.0000
10	2.6107	0.0000	0.0000	0.0000	0.0000
11	1.6065	0.0000	0.0000	0.0000	0.0000
12	1.0203	2.1139	28.0592	2.1139	2.2007
13	0.6302	11.2429	48.1164	9.1290	3.6255
14	0.4068	17.7557	13.4294	6.5128	1.0780
15	0.2530	25.4730	6.4914	7.7173	0.4940
16	0.1635	32.3837	2.2980	6.9107	0.1847
17	0.0996	39.7830	0.9936	7.3994	0.0733
18	0.0624	46.3854	0.3341	6.6024	0.0257
19	0.0405	52.9878	0.1339	6.6023	0.0108
20	0.0252	64.8133	0.0985	11.8256	0.0075
21	0.0161	75.6506	0.0355	10.8373	0.0028
22	0.0099	81.9744	0.0083	6.3238	0.0006
23	0.0062	84.7550	0.0014	2.7806	0.0001
24	0.0037	86.3320	0.0003	1.5770	0.0000